HHS Public Access

Author manuscript

Cell Host Microbe. Author manuscript; available in PMC 2024 December 13.

Published in final edited form as:

Cell Host Microbe. 2023 December 13; 31(12): 2007–2022.e12. doi:10.1016/j.chom.2023.10.016.

Fiber-Deficient Diet Inhibits Colitis through Regulation of the Niche and Metabolism of a Gut Pathobiont

Peter Kuffa[1], **Joseph M. Pickard**[1], **Austin Campbell**[2], **Misa Yamashita**[3], **Sadie R. Schaus**[2], **Eric C. Martens**[2], **Thomas M. Schmidt**[2], **Naohiro Inohara**[1], **Gabriel Núñez**[1,5], **Roberta Caruso**[1,4,5,*]

[1]Department of Pathology and Rogel Cancer Center, the University of Michigan Medical School, Ann Arbor, MI 48109, USA.

[2]Department of Microbiology and Immunology, the University of Michigan Medical School, Ann Arbor, MI 48109, USA.

[3]Department of Public Health and Preventive Medicine, Yamaguchi University Graduate School of Medicine, Ube, Yamaguchi 755-8505, Japan.

[4]Lead contact

[5]Senior author

SUMMARY

Exclusive enteral nutrition (EEN) with fiber-free diets is an effective steroid-sparing treatment to induce clinical remission in children with Crohn's disease (CD). However, the mechanism underlying the beneficial effects of EEN remains obscure. Using a model of microbiota-dependent colitis with the hallmarks of CD, we find that administration of a fiber-free diet prevents the development of colitis and inhibits intestinal inflammation in colitic animals. Remarkably, fiber-free diet alters the intestinal localization of *Mucispirillum schaedleri,* a mucus-dwelling pathobiont, which is required for triggering disease. Mechanistically, the absence of dietary fiber reduces nutrient availability and impairs the DNRA metabolic pathway of *M. schaedleri,* leading to exclusion from the mucus layer and disease remission. Thus, appropriate localization of the specific pathobiont in the mucus layer is critical for disease development, which is disrupted by fiber exclusion. These results suggest strategies to treat CD by targeting the intestinal niche and metabolism of disease-causing microbes.

Graphical Abstract

*Correspondence: rocaruso@med.umich.edu.

AUTHOR CONTRIBUTIONS

R.C and G.N. conceived and designed experiments. P.K. and R. C. conducted most of the experiments with help by J. M. P., A.C. and S. R. S. E. C. M., and T. M. S. provided advice, discussion, and critical materials. N.I. and M.Y. performed bioinformatics analyses. R.C. and N. I. analyzed the data. R.C. and G. N. wrote the manuscript with contributions from all authors.

DECLARATION OF INTERESTS

The authors declare no competing financial interests.

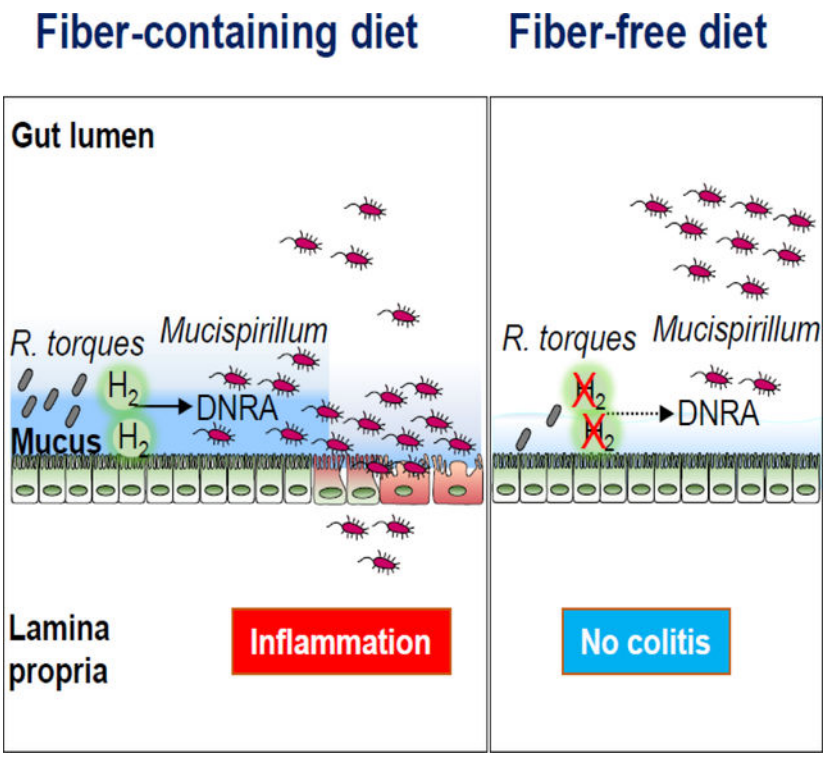

eTOC Blurb

Kuffa et al. demonstrate that fiber-free diet prevents and inhibits disease in a Crohn's disease-like colitis model. Fiber exclusion reduces the abundance of *M. schaedleri,* a mucus-dwelling pathobiont required for triggering disease. Mechanistically, fiber deprivation reduces nutrient availability and impairs the DNRA metabolic pathway in *M. schaedleri* to promote re-localization.

Keywords

Crohn's disease; exclusive enteral nutrition; fiber-free diet; mucus-dwelling pathobiont; dissimilatory nitrate reduction to ammonia; *Ruminococcus torques* ; *Mucispirillum schaedleri*

INTRODUCTION

Crohn's disease (CD), one of the major forms of inflammatory bowel disease (IBD), is a chronic inflammatory disorder of the gastrointestinal tract that affects both children and adults [1,2]. While the incidence of adult-onset IBD has plateaued in many westernized regions [3,4], the IBD incidence in children including very early onset IBD (VEOIBD) has increased in the Western world over the past two decades, with a more pronounced increase in CD [5,6]. Although the pathogenesis of CD remains poorly understood, accumulating evidence suggests that CD arises from a confluence of genetic and environmental factors that alter gut homeostasis [1,7]. Genetic studies have identified mutations in more than 100 genes that are associated with CD, many of which regulate microbial recognition, killing, and immune responses to microbes [8,9]. Furthermore, increased genetic burden has been associated with earlier age of onset for CD including VEOIBD [10]. Both VEOIBD and adult

CD are associated with mutations in *NOD2,* a gene that regulates bacterial recognition, and genes that encode components of the phagocyte NADPH oxidase complex including CYBB that are critical for bacterial killing [7,11,12]. Notably, NOD2 deficiency together with deficiency in CYBB triggers spontaneous early-onset CD-like colitis in mice exposed to a specific microbiota [13]. Thus, specific interactions between host genes and the microbiota are critical for the development of disease.

Alterations in the gut microbiota or dysbiosis are commonly found in patients with IBD including CD [7]. For instance, a decreased community diversity and a shift in certain bacterial taxa is a common feature of the disease in both adults and children with CD [7,14]. However, such microbial alterations seen in CD patients may be secondary to inflammation. Although direct evidence for a causal role for specific microbes in CD is lacking, the imbalance in the gut microbial community towards a dysbiotic state is more pronounced in mucosal samples than in the stool of adult CD and treatment-naïve pediatric CD patients [14,15]. Thus, it is conceivable that mucus-dwelling microbes, due to their proximity to the intestinal epithelium, are more likely to trigger abnormal mucosal immune responses in genetically susceptible individuals. Thus, strategies that target disease-causing microbes living near the epithelium may be beneficial in patients with CD.

Given the potential importance of the gut microbiota in triggering CD, the development of therapeutic approaches that target causal intestinal microbes may provide a unique approach to treatment of this disease. Diet is one of the available tools that can be used to modify the intestinal microbiota [7]. As of now, there are no clear evidence-based recommendations for diet as therapy for CD, except for EEN. EEN is a complete liquid formula diet that contains all nutritional requirements but is typically free of or low in plant fiber [16,17]. EEN is a first line therapy for mild to moderately active pediatric CD, providing complete nutrition while simultaneously inducing remission in 60–85% of cases [18–20]. EEN is also effective in select adult patients with CD [21]. However, EEN is a very restrictive diet, which has limited its acceptability and clinical use, particularly in adults with CD. The effectiveness of EEN in the treatment of pediatric CD is somewhat unexpected, given that the administration of low fiber diets in murine models is associated with thinning of the mucus layer and increased mucus permeability [22–24]. The mechanism by which EEN induces clinical remission in children with CD remains unclear, although it has been suggested that EEN may act by reducing the luminal load of dietary antigens or altering the composition of the gut microbiota [25,26]. Using a spontaneous model of CD, we found that a fiber-free diet ameliorates colitis by altering the intestinal localization of a specific gut pathobiont that is required to trigger CD-like disease in genetically susceptible mice. Mechanistically, fiber-free diet inhibited the ability of mucin-degrading microbes to supply critical molecules that are required for the metabolism and maintenance of the disease-causing pathobiont in the mucus layer.

RESULTS

Exclusion of dietary fiber inhibits spontaneous CD-like colitis

To investigate the role of dietary fiber in intestinal inflammation, we utilized a spontaneous model of CD-like colitis. In this model, mice doubly deficient in Nod2 and

phagocyte NADPH oxidase/Cybb (DKO), two genes associated with human CD, develop a spontaneous early-onset Th1-type CD-like colitis when exposed to Taconic microbiota (Tac) [13]. To determine whether dietary fiber prevents the development of colitis, littermate Tac-DKO mice were separated at weaning before the development of colitis and fed *ad libitum* a fiber-containing mouse chow, referred to as regular chow (RC), or a fiber-deficient diet (FD) for up to 9 weeks (Figure 1A). The macronutrient composition of FD resembles some low fiber/no fiber EEN diets clinically used in pediatric CD patients for up to 12 weeks to induce disease remission [17,18,25]. First, we monitored diet consumption and found no difference between the RC and the FD (Figure S1A). Tac-DKO mice maintained on the RC spontaneously developed CD-like colitis, as verified by increased levels of fecal lipocalin-2 (Lcn-2) (Figure 1B), a marker of intestinal inflammation [27], and by histological examination (Figures 1C and 1D). Consistent with our previous study [13], gut inflammation in RC-fed Tac DKO mice was characterized by crypt architectural distortion, transmural inflammatory cell infiltrates, and ulcers (Figure 1C), all hallmarks of CD in both adults and children [1,28]. In contrast, Tac-DKO animals maintained on FD were protected from colitis (Figures 1B–D). Consistent with these observations, transcript levels of pro-inflammatory cytokines, such as tumor necrosis factor α (TNFα), interferon γ (IFNγ), interleukin-6 (IL-6), but not IL-17A, were decreased in colonic explants of Tac-DKO mice on FD as compared to the animals maintained on RC (Figure 1E).

The RC and FD diets differ substantially in several aspects of their macronutrient composition in addition to fiber. To specifically test the influence of fiber on disease severity, we utilized a custom-made control mouse diet (CTR), in which roughly 50% of the simple sugar FD contains (glucose) was removed and replaced by several natural fiber sources to match the percentage of neutral detergent fiber present in RC (Table S1). In a preventive protocol, littermate Tac-DKO mice were fed either the CTR or the FD, before the development of colitis (at 21 days of age), up to 9 weeks (Figure S1B). While no difference in food consumption was noted between the two groups (Figure S1C), restoring dietary fiber using the CTR diet to Tac-DKO mice promoted the development of colitis, as confirmed by Lcn-2 measurements, histological examination, and pro-inflammatory cytokine profiles (Figures S1D–G).

Next, we examined the therapeutic impact of fiber exclusion on mice that had already developed gut inflammation. In these studies, littermate colitic Tac-DKO mice (4–5 weeks of age) were separated and fed either the RC or the FD for up to 7 weeks. Notably, Tac-DKO mice on FD exhibited decreased Lcn-2 levels and histology compared to mice maintained on RC (Figures 1F–H). Collectively, these results indicate that exclusion of fiber from the diet inhibits intestinal inflammation in our model of CD-like colitis using both preventive and therapeutic protocols.

Fiber-deficient diet reduces the abundance of pathobiont *Mucispirillum* in the mucus layer

Administration of a FD results in thinning of the intestinal mucus layer, which is associated with increased mucin-degrading activity of mucus-dwelling symbionts [22,23,29]. Consistent with these observations, FD-fed Tac-DKO mice displayed increased permeability to FITC-dextran (Figure S2A) and reduced mucus thickness compared to their RC-fed (Figures 2A–

C) or CTR-fed (Figure S2C) animal counterparts. Similar thinning of the colonic mucus layer was observed in colitic Tac DKO mice fed the FD in contrast to RC-fed littermates (Figure S2B). As expected, degradation of the mucus layer during periods of fiber exclusion brought luminal microbes closer to the gut epithelium (Figures 2A and 2B, right panels). Next, we examined whether mucus production was altered in Tac-DKO mice fed the FD. To this end, we determined the abundance of transcripts encoding several key proteins involved in synthesis and regulation of the mucus layer, such as Muc2, Muc5ac, Tff1, Tff3, and Klf3 [30]. Our results show no differences in transcript levels of any genes examined between FD and RC groups (Figure 2D). Consistent with these findings, qualitative visualization by Alcian blue and Alcian blue/Periodic acid-Schiff (PAS) staining showed that the colonic tissue of FD- and RC-fed Tac DKO mice contained similar numbers of goblet cells (Figures 2A and 2B, first two panels from the left). Despite displaying reduced mucus layer thickness (Figure 2C), the FD-fed Tac-DKO showed less inflammation compared to the RC group (Figures 1B–D).

Colitis in Tac-DKO mice is triggered by intestinal accumulation and penetration of the pathobiont *Mucispirillum schaedleri* (referred here as *Mucispirillum*) [13]. We thus examined the intestinal abundance of *Mucispirillum* during dietary intervention. Surprisingly, time-course analysis revealed increased luminal *Mucispirillum* abundance in fecal samples obtained from FD-fed Tac-DKO mice compared to RC-fed animals at later time points (i.e., 7 and 9 weeks of dietary intervention) (Figure 2E). These results were somewhat unexpected given that FD-fed Tac-DKO were protected from the development of colitis (Figure 1). Because *Mucispirillum* primarily localizes to the mucus layer [31], we set out to quantify *Mucispirillum* abundance in the mucus layer during dietary interventions. Remarkably, we found that unlike the RC-fed Tac-DKO mice whose mucus layer was enriched with *Mucispirillum*, FD-fed animals exhibited a marked reduction of *Mucispirillum* abundance in the mucus layer (Figure 2F), despite having similar bacterial genome copies (16S rRNA) and host genomic copy numbers (ActB) in both luminal and mucosal compartments (Figures S2D and S2E). In line with these findings, *Mucispirillum* accumulated in the proximity of the gut epithelium in RC-fed mice, whereas the bacterium in FD-fed animals primarily localized in the intestinal lumen in FD-fed animals, as shown by fluorescence in situ hybridization (Figures 2G and 2H). Taken together, these results indicate that the absence of dietary fiber leads to altered localization of the disease-causing *Mucispirillum* in the intestine.

The mucus layer is critical for *Mucispirillum* intestinal colonization and colitis induction

Mucispirillum was barely detectable in the mucus layer of FD-fed Tac-DKO mice (Figure 2F), which were protected from disease development (Figures 1B–D). Thus, we hypothesized that appropriate localization of *Mucispirillum* in the mucus layer is critical for its ability to locally invade the intestinal tissue and to trigger inflammation. To test this hypothesis, adult littermate DKO mice harboring *Mucispirillum*-free microbiota (microbiota from Jackson Laboratory (Jax) mice) [13], were fed either the RC or the FD for two weeks prior to bacterial challenge (Figure 3A). While remaining on either the RC or the FD, Jax-DKO mice were pre-treated with vancomycin and then orally gavaged with *Mucispirillum* (Figure 3A). As expected, the absence of dietary fiber resulted in reduced

mucus thickness in Jax-DKO mice (Figure 3B and Figure S3A). Notably, *Mucispirillum* colonized RC-fed Jax-DKO mice over time after gavage, while its intestinal colonization was markedly reduced in FD-fed animals (Figure 3C). In line with these observations, oral challenge with *Mucispirillum* resulted in weight loss (Figure 3D) and colitis as determined by increased levels of fecal Lcn-2 in RC-fed mice, but not in FD-fed DKO animals (Figure 3E). Histological examination of *Mucispirillum*-colonized mice confirmed the development of colitis in RC-fed DKO mice, which was inhibited in FD-fed animals (Figures 3F and 3G). To further test the role of the mucus layer in *Mucispirillum* colonization, we utilized *Muc2*$^{-/-}$ mice that are deficient in Muc2, the dominant colonic mucin glycoprotein. Consistent with previous evidence [32], *Muc2*$^{-/-}$ mice show a very thin colonic mucus layer (Figure S3B and S3C). Littermate mutant *Muc2*$^{-/-}$ and heterozygous *Muc2*$^{+/-}$mice were pre-treated with vancomycin and then orally gavaged with *Mucispirillum* (Figure 3H). Because *Muc2*$^{-/-}$ mice can develop colitis over time [33], we used young mice and performed a short bacterial challenge in *Muc2*$^{-/-}$ animals to avoid confounding effects of inflammation on *Muscispirillum* colonization (Figure 3H). The *Muc2*$^{-/-}$ and *Muc2*$^{+/-}$ mice were euthanized 1 day after bacterial gavage, when levels of fecal Lcn-2 were low and comparable between both groups of mice (Figure 3I). At this time point, *Muc2*$^{-/-}$mice exhibited a very thin mucus layer, and a loss of Alcian-blue-positive goblet cells, compared to *Muc2*$^{+/-}$ animals (Figure 3J and S3D). Notably, *Mucispirillum* colonization was markedly reduced in *Muc2*$^{-/-}$mice compared to their heterozygous littermates (Figure 3K). Collectively, these results indicate an intact mucus layer is important for *Mucispirillum* intestinal colonization.

We also sought to assess the role of FD and the mucus layer in maternal transmission of *Mucispirillum*. To this end, we modified our protocol to perform dietary interventions during the neonatal period by feeding pregnant Tac-DKO dams either the RC or the FD, which allows pups to be exposed to different diets from birth (Figure 3L). Jax-DKO dams fed either the RC or the FD were included as controls (Figure 3L). As expected, fiber exclusion resulted in thinning of the mucus layer in both Tac-DKO (Figure 3M) and Jax-DKO pups (Figure 3N). In line with previous evidence [22], switching to the FD induced a microbiota shift in favor of the mucin-degrading species, such as *Akkermansia muciniphila*, in Jax-DKO pups (Figure 3O). In contrast, the mucus-dwelling *Mucispirillum* was depleted in Tac-DKO pups in response to low fiber administration compared to RC-fed pups (Figure 3O). Consistent with the inability of *Mucispirillum* to colonize the mucus layer in the absence of dietary fiber, FD-fed Tac-DKO pups did not develop spontaneous colitis (Figures S3C–E). In contrast, *Mucispirillum*-colonized RC-fed Tac-DKO pups spontaneously developed intestinal inflammation, as assessed by fecal Lcn-2 levels and histological examination (Figures S3E–G). As expected, Jax-DKO pups, whose microbiota is devoid of *Mucispirillum* [13], did not develop intestinal inflammation regardless of the diet (Figures S3H–J). These results indicate that diet-induced alteration of the mucus layer affects vertical transmission of *Mucispirillum*. Collectively, these results indicate that appropriate localization of *Mucispirillum* in the mucus layer is critical for its ability to trigger intestinal inflammation.

R. torques promotes *Mucispirillum* growth

Since our data indicate that the mucus layer plays a crucial role in *Mucispirillum* colonization (Figure 3), we next assessed the ability of *Mucispirillum* to grow in BHI medium in the presence of different sugars using a custom carbohydrate array that contains most of the common mono- and polysaccharides present in plant and animal tissue, including purified mucin *O*-glycans [22]. Unlike *Escherichia coli*, which exhibited optimal growth on monosaccharides (Figure 4A and Table S2), *Mucispirillum* grew poorly in BHI medium supplemented with either mono- or polysaccharides (Figure 4A and Table S2), while the bacterium grew in a dose-dependent manner in the presence of either amino acids or glycerol (Figure S4A). Taken together, our results suggest that *Mucispirillum* is not a primary degrader of dietary fiber and/or host-derived polysaccharides. Thus, we reasoned that *Mucispirillum* may utilize breakdown products produced by mucus-degrading microbes. To test this hypothesis, we utilized specific-pathogen free (SPF) and germ-free (GF) C57BL/6 mice and fed them either the RC or the FD for 2 weeks. Sterile supernatants were prepared anaerobically from luminal contents and mucus isolated from the ceca of RC- and FD-fed SPF and GF C57BL/6 mice and used as a medium for either *Mucispirillum* or *E. coli* growth. *E. coli* bloomed in the presence of GF-derived, but not SPF-derived, supernatants regardless of the diet (Figure S4B), suggesting that *E. coli* and intestinal microbes compete for nutrients needed for growth. In contrast, *Mucispirillum* growth was slightly supported by GF-derived supernatants, but markedly enhanced by SPF-derived supernatants, particularly by the cecal supernatant from SPF mice fed the FD (Figure 4B). Taken together, these results indicate that *Mucispirillum* growth is promoted by nutrients provided by intestinal microbes.

To examine the bacterial species that are affected by the exclusion of dietary fiber, we analyzed the composition of the gut microbiota in Tac-DKO mice over time. The α diversity in the fecal microbiota of RC-fed and the FD-fed Tac-DKO mice remained comparable, except for week 7 after dietary intervention (Figure S4C). Likewise, no α diversity differences were noted in the fecal microbiota of CTR- vs FD-fed Tac-DKO mice, except for week 3 (Figure S4D). Importantly, fecal microbiota composition significantly differed among the three diet groups (Figure 4C). As expected, a decrease in the abundance of fiber-degrading species (i.e., Porphyromonadaceae) was observed in the absence of fiber (Figure 4D and Table S3). Moreover, the abundance of several species in the Lachnospiraceae family varied markedly between mice fed fiber-containing diets (either RC or CTR) and a FD diet as determined by linear discriminant analysis effect size (LEfSe) analysis ($p < 0.05$) (Figure 4D and Table S3). While specific Lachnospiraceae species were reduced in the FD group, other Lachnospiraceae species were increased in the absence of dietary fiber (Figure 4D and Table S3). Furthermore, 16S rRNA sequence alignment homology analysis revealed that the Lachnospiraceae species whose abundance decreased after fiber deprivation (Figure 4D), were similar to that of *Ruminococcus torques* (Figure S5A), a well-characterized member of the Lachnospiraceae family [34]. We thus assessed whether the growth of *Mucispirillum* is promoted by *R. torques*. Consistent with previous evidence [35], we found that *R. torques* was able to grow on purified rectal glycoproteins which was not affected by the presence of *Mucispirillum* (Figure S5B). To assess whether mucin-degrading *R. torques* regulates the growth of *Mucispirillum*, we co-cultured *R. torques* and *Mucispirillum* in the presence of

purified rectal glycoproteins or monosaccharides (i.e., glucose and rhamnose). We found that *R. torques* enhanced *Mucispirillum* growth in the presence of mucin-containing, but not in mucin-free, medium (Figure 4E). Additionally, GF C57BL/6 mice monocolonized with R. *torques* or non-mucin degrading *E. coli* as a control were fed a RC (Figure S5C and S5D). Monocolonization with *R. torques* did not affect the intestinal mucus thickness (Figure S5E). We found that supernatants derived from *R torques*-monocolonized mice enhanced the growth of *Mucispirillum in vitro* compared to supernatants derived from either GF or *E. coli*-monocolonized animals (Figure 4F). Likewise, the intestinal colonization of *Mucispirillum* was increased after gavage into *R. torques*-monocolonized mice when compared to gavage of the bacterium into GF or *E. coli*-monocolonized mice (Figure 4G). Thus, dietary fiber exclusion alters the abundance of specific members of the Lachnospiraceae family that can promote the growth of *Mucispirillum*.

Exclusion of dietary fiber affects the DNRA metabolic pathway in *Mucispirillum*

The exclusion of fiber from the diet led to a relocation of *Mucispirillum* from the mucus layer to the luminal compartment (Figures 2E and 2F). We reasoned that reduced abundance of *Mucispirillum* in the mucus layer may be the result of altered metabolism of the bacterium at that site after administration of a fiber-free diet. To assess this, we performed metatranscriptomic analysis to identify *Mucispirillum* genes differentially expressed in the intestine of mice maintained on RC compared to animals fed the FD. Our transcriptomic analysis revealed 8 *Mucispirillum* genes that were more abundant and 2 genes less abundant in RC-fed mice compared to FD-fed animals (Figure 5A and Table S4). Of these genes, only 2 genes, *nroB* and *nroD*, have been functionally annotated in an operon we named *nro* (nitrate reductase operon) in the *Mucispirillum* genome and predicted to act in the metabolic pathway of dissimilatory nitrate reduction to ammonia (DNRA) (Figure S6), a part of anaerobic respiration [36]. *Mucispirillum* can utilize nitrate, which is abundant in the inflamed gut [37], as an electron acceptor, and hydrogen (H_2) as an electron donor for anaerobic respiration [38]. To test whether *Mucispirillum* was capable of DNRA, we incubated the bacterium in enriched brain heart infusion (BHI) with different combinations of nitrate and/or H_2 under anaerobic conditions. Nitrate increased *Mucispirillum* growth in the presence of H_2 (Figure 5B), which was associated with H_2 consumption and ammonium production (Figures 5C and 5D), indicating that *Mucispirillum* was indeed capable of DNRA under our growth conditions. Further transcriptomic analysis revealed reduced expression of all genes belonging to the unique DNRA-associated nitrate reductase operon (*nroA*, *nroB*, *nroC*, *nroD*, *nroE* and *nroF*) in the mucus layer of FD-fed Tac-DKO mice compared to RC-fed animals (Figure 5E and 5F, and Table S4). Taken together, these results suggest that the exclusion of dietary fiber decreases within the mucus layer the function of DNRA, a metabolic pathway that promotes *Mucispirillum* growth.

Fiber exclusion alters fermentative H_2 metabolism and interspecies H_2 transfer

H_2 fuels *Mucispirillum* growth in the presence of nitrate (Figure 5B), but *Mucispirillum* lacks hydrogenases that are required for H_2 production [38]. Thus, we hypothesized that H_2 is provided to *Mucispirillum* by fermentative microbes, which may be impaired in mice fed a FD. We thus surveyed the distribution of hydrogenase-encoding genes that leads to the production of diffusible H_2 in Tac-DKO mice to determine the dominant mechanisms

of H_2 cycling during dietary fiber exclusion. Two distinct classes of hydrogenases, FeFe Groups A1 and B and NiFe Group 4a, are involved in hydrogenogenic fermentation [39]. Transcriptomic analysis revealed a reduction in the total transcript levels of FeFe Groups A1 and B hydrogenase homologues in the mucus layer of Tac-DKO mice that were fed the FD compared to mice maintained on RC (Figure 6A and Table S5). In contrast, no changes in the transcript levels of these hydrogenases were found in the luminal compartment (Figure 6A and Table S5). These results suggest that H_2 production is diminished in the mucus layer after dietary fiber exclusion. Furthermore, we found that distinct members of the Lachnospiraceae family harboring [FeFe]-hydrogenase genes were differentially abundant in each diet group (i.e., RC *vs* FD) and in each intestinal compartment (i.e., mucus *vs* lumen) (Figure 6B and Table S5). We also assessed H_2 metabolism in the human gut during fiber exclusion by analyzing available metagenomics data from pediatric CD patients who received EEN [26]. A marginal increase in the number of microbes (relative abundance) encoding FeFe Groups A1 and B hydrogenases was observed in fecal samples isolated from EEN-treated CD children (1 week of EEN) compared to samples of patients before starting EEN (Figure 6C and Table S6). More importantly, consistent with our mouse transcriptomic data (Figure 6B), we found that distinct members of the Lachnospiraceae family harboring [FeFe]-hydrogenase genes were differentially abundant in CD children before starting EEN (baseline) and after 1 week of nutritional therapy (Figure 6D and Table S6). Thus, our findings indicate that the exclusion of dietary fiber alters the levels of Fe-Fe hydrogenases-expressing Lachnospiraceae both in mice and in humans with CD.

We tested whether *Mucispirillum* utilizes H_2 produced by Lachnospiraceae species to promote its growth. In these experiments we utilized *R. torques,* which can enhance *Mucispirillum* growth (Figures 4E and 4F), and tested if *R. torques* can promote *Mucispirillum* growth by transferring H_2. To this end, we first confirmed that *R. torques* grew (Figure S7A) and produced H_2 in nitrate-supplemented BHI medium (Figure 6E). Next, we co-cultured *Mucispirillum* with *R. torques* in the absence of exogenous H_2 in nitrate-supplemented BHI. Notably, *R. torques* promoted *Mucispirillum* growth in the absence of H_2 to the same extent as it was observed in the presence of exogenous H_2 (Figure 6F). The enhancement of *Mucispirillum* growth by *R. torques* was associated with ammonium production (Figure 6G), suggesting that *Mucispirillum* uses anaerobic respiration through DNRA in the presence of *R. torques*. We next examined whether *R. torques* promotes *Mucispirillum* growth through H_2 cross-feeding. To this end, we utilized a nitrogen sparging technique that has been shown to decrease the dissolved H_2 concentration in a fermentative H_2-producing reactor [40]. In these experiments co-cultures of *R. torques* and *Mucispirillum* were grown in bioreactor vessels and sparged with a mixed gas containing 20% carbon dioxide (CO_2) and either 80% nitrogen (N_2) or 80% H_2 (Figure S7B). N_2 sparging resulted in a marked reduction of dissolved H_2 in the bacterial co-cultures (Figure 6H) that was stable over a 3-day culture period (Figure S7C). N_2 sparging resulted in a marked reduction of *Mucispirillum* growth compared to the H_2-sparged cultures (Figure 6I), which is consistent with a reduced H_2 concentration (Figure 6H and Figure S7C). Taken together, these results suggest that Lachnospiraceae species play an important role in H_2 metabolism, both in the mouse and human colon, during periods of fiber exclusion.

Furthermore, Lachnospiraceae species, such as *R. torques,* can support the growth of disease-causing *Mucispirillum* via interspecies H_2 transfer.

DISCUSSION

The gut microbiota is thought to be a crucial determinant of host susceptibility to several diseases, including CD [41]. Although dietary fiber is typically considered beneficial in humans [42], fiber-free (or fiber-low) diet therapies such as EEN markedly improve disease outcomes in children with CD [18–20]. Consistent with the human data, our findings indicate that the administration of a fiber-free diet prevents and/or ameliorates the CD-like colitis in our animal model that is based on mutations associated with human disease. The mechanism by which EEN is effective in inducing clinical remission in pediatric CD remains unknown, but it has been proposed that EEN may act by reducing the amounts of dietary antigens or changing the composition of the gut microbiota [25,26]. Our results reveal a distinct and unique mechanism through which the absence of dietary fiber inhibits intestinal inflammation by targeting the localization and metabolism of the pathobiont *Mucispirillum* that is required for triggering colitis in our model [13]. Mucus-inhabiting microbes such as *Mucispirillum* live near the intestinal epithelium and thus are well positioned to locally penetrate into the lamina propria to trigger intestinal inflammation [35,43]. Beside the proximity to the gut epithelium, *Mucispirillum* harbors some virulence traits, including a type VI secretion system and putative effector proteins [38]. Such bacterial features may lower the threshold for local penetration increasing the ability of *Mucispirillum* to trigger colitis when host protective antimicrobial mechanisms are compromised by IBD-associated mutations, such as NOD2 and CYBB.

Our results show that localization in the mucus layer, and not abundance in the intestinal lumen, is critical for *Mucispirillum* to trigger inflammation. Although these findings provide a plausible mechanism to account for the efficacy of EEN in pediatric CD, further studies are needed to determine whether the beneficial effect of EEN is mediated via a similar mechanism in human CD. Although EEN remains the most validated nutritional recommendation for inducing remission in CD, there are some challenges to the use of EEN, especially in adults, due to its poor palatability. In this context, the use of a fiber-free food-based diet, with similar composition to EEN [44], might represent a more acceptable dietary treatment particularly in adults in whom EEN compliance is low, and may raise the prospect of long-term dietary maintenance therapy in CD.

Members of the Lachnospiraceae family, a subgroup of Clostridia cluster XIVa [34], were most responsive to our dietary intervention with fiber-free diet. Although Lachnospiraceae species can utilize plant pectin, some Lachnospiraceae species can degrade and utilize mucin for growth [34]. It is, therefore, not surprising that some Lachnospiraceae species were abundant in mice fed a fiber-containing diet, while the abundance of other species of the same family were more abundant in animals fed a fiber-free diet. Although Lachnospiraceae are among the main producers of short-chain fatty acids, such as butyrate, which promote intestinal barrier function, different taxa of Lachnospiraceae are also associated with intestinal disease. For instance, mucin-degrading *R. torques* and *R. gnavus* are two Lachnospiraceae species particularly abundant in CD patients [43,45]. Furthermore,

R torques is also more frequently found in the gut of relatives of patients with CD that harbor a dysbiotic microbiota [46]. Most importantly, a recent prospective cohort study of individuals at risk of developing CD revealed that mucolytic *R. torque*s is the top important taxon associated with the future onset of CD, suggesting that *R. torques* can be an important contributor to CD development [47]. Indeed, we show that mucolytic *R. torques* enables the pathobiont *Mucispirillum* to acquire host-derived nutrients required for its growth. *R. torques* produce H_2, a fermentation byproduct, which, in turn, supports *Mucispirillum* growth. Our findings indicate that fiber exclusion reduces the expression of hydrogenases in the mucus layer and alters the levels of hydrogenase-expressing Lachnospiraceae. Thus, the absence of dietary fiber affects the activity of fermentative bacteria (hydrogenogens), which, in turn, limit nutrient availability necessary for *Mucispirillum* colonization in the mucus layer. Notably, our findings indicate that fiber-free EEN alters H_2 metabolism in CD children, suggesting that one potential beneficial effect of fiber-free therapy in CD might be linked to reduced H_2 availability to gut pathobionts such as *Mucispirillum* that depend on mucolytic microbes for survival at the mucus layer. Overall, our studies provide the concept that diet can control the proximity of the pathobionts to the host epithelium through mucolytic microbes that promote their metabolism and growth at the mucus layer.

Our transcriptomic data reveal a unique metabolic pathway, DNRA, utilized by *Mucispirillum* that was reduced in the mucus layer by dietary fiber exclusion. *Mucispirillum* can grow in the presence of nitrate and H_2, as it can utilize nitrate as an electron acceptor and H_2 as an electron donor in the context of the DRNA pathway. Importantly, our findings could be broadly applied to other gut pathobionts that use anaerobic respiration. In line with this, Proteobacteria take advantage of more abundant electron acceptors allowing respiration, such as nitrate, produced in the inflamed gut to bloom during periods of active IBD [37]. Consequently, targeting the molybdenum cofactor-dependent enzymes that are required by some nitrate-utilizing pathogenic bacteria for anaerobic respiration protects mice from colitis by blunting the expansion of pathogenic Enterobacteriaceae [48]. Our studies further highlight the importance of identifying metabolic pathways utilized by pathobionts to promote their colonization and demonstrate the feasibility of a dietary approach to target these metabolic pathways as a therapeutic strategy for the treatment of CD.

STAR★METHODS

RESOURCE AVAILABILITY

Lead Contact—Further information and requests for resources and reagents should be directed to and will be fulfilled by the Lead Contact, Roberta Caruso (rocaruso@med.umich.edu).

Materials availability—Any newly generated items in this work will be shared on request.

Data and code availability—Raw data files for 16S and metatranscriptomics sequencing are freely available at BioProject database, ID number: PRJNA984252. This paper does not report original code. Any additional information required to reanalyze the data reported in this work paper is available from the lead contact upon request.

EXPERIMENTAL MODEL AND STUDY PARTICIPANT DETAILS

Animals and diet treatments—All animal experiments followed protocols approved by the University of Michigan, Institutional Animal Care and Use Committee (IACUC).

Three- to eight-week-old female and male SPF mice were used. The SFP C57BL/6J animals were purchased from the Jackson Laboratory (JAX: 000664). SPF doubly-deficient *Nod2/Cybb* mice harboring microbiota from either Taconic Biosciences or Jackson Laboratory previously described [13] were housed in the Animal Facility at the University of Michigan. SPF *Muc2*$^{-/-}$ on a C57BL/6J background were provided by E. C. Martens (University of Michigan) and originally obtained from Dr. Leonard Augenlicht (Albert Einstein College of Medicine) [49]. Eight- to twelve-week-old female and male GF C57BL/6NTac mice (from Taconic Biosciences, B6-F; B6-M) were housed in flexible film isolators at the University of Michigan Germ-Free Mouse Facility. The absence of microbes in GF mice was verified weekly by aerobic and anaerobic microbial culture and microscopic analysis of stained cecal contents. Mice were housed in groups as appropriate for gender, litter and diet requirements, and provided *ad libitum* with autoclaved distilled water and the diets described below.

The fiber-deficient (FD) diet (TD.130343) was manufactured by Teklad/Envigo (Indianapolis, IN) and, as previously described [22], consisted of a modified version of Harlan TD.08810, in which starch and maldodextrin were replaced with glucose. The custom-made control diet (CTR) (TD.190428, Teklad/Envigo, Indianapolis, IN) was designed in collaboration with a nutritionist at Envigo. It is a version of the FD diet from which roughly 50% of the simple sugar content (glucose) was removed and replaced by several natural fiber sources, including wheat middlings, alfalfa meal, wheat germ, beet pulps and oats. Additionally, to account for protein and fat coming from natural ingredients, casein and corn oil were reduced in the CTR diet to keep protein at 23.8% (26.3% kcal) and fat at 15.3% by weight (38.0% kcal), as in the FD diet (Table S1). FD and CTR diets were sterilized by gamma irradiation and regular chow (RC) (LabDiet 5L0D, laboratory rodent diet, LabDiet, St. Louis, MO) was sterilized by autoclaving. GF mice were fed regular chow (LabDiet 5013, rodent breeder diet, LabDiet, St. Louis, MO) that had also been sterilized by autoclaving. Daily food consumption amount per mouse in each cage was calculated. Mice of similar age and similar weight were randomly assigned to experimental groups. None of the animal experiments were blinded except for the pathology assessment and mucus thickness measurement.

Trio breeding strategy—Eight- to twelve-week-old doubly-deficient *Nod2/Cybb* mice, harboring microbiota from either Taconic Biosciences or Jackson Laboratory, were used to set up trio breeding cages, consisting of one male and two females maintained on RC. At embryonic day 14–16, pregnant dams were separated, single-housed and either switched to FD diet or maintained on RC for the duration of the experiments.

Bacteria—*Mucispirillum schaedleri* isolated from the mouse cecum was a gift from Jani L. O'Rourke (The University of New South Wales, Sydney, Australia) [31]. *E. coli* K12 strain BW25113 was originally received from Yale Coli Genetic Stock Center (https://

cgsc.biology.yale.edu/). *Ruminococcus torques* strain VIII was provided by E. C. Martens (University of Michigan), and originally isolated and characterized by L.C. Hoskins [50].

METHOD DETAILS

Bacterial cultures—*Mucispirillum* was grown anaerobically in enriched Brain Heart Infusion (BHI) (plate and/or broth), which contained 37 g/l BHI (BD Difco, Franklin Lakes, NJ), 5 g/l yeast extract (Sigma-Aldrich, St. Louis, MO), 0.5 g/l l-cysteine (Sigma, St. Louis, MO), and added 2ml vitamin K3 (menadione, 1mg/ml stock concentration, Sigma, St. Louis, MO), 4 ml hematin/l-histidine solution (1.9mM hematin/0.2M l-histidine stock concentration, both from Sigma, St. Louis, MO), 16 g/l agar (only added to the plates) (BD Difco, Franklin Lakes, NJ), 5% new born calf serum (Gibco, Thermo Fisher Scientific, Waltham, MA), 5% horse serum (Gibco, Thermo Fisher Scientific, Waltham, MA) and 5% sheep serum (Sigma, St. Louis, MO). For *Mucispirillum* carbohydrate growth array, we used a BHI broth, which was made as described above except for the absence of glucose (we used a dextrose-free BHI (MyBiosource, San Diego, CA)) and for the absence of the three sera. *E. coli* was grown overnight in LB medium (10 g/l peptone, 5 g/l yeast extract, 10 g/l sodium chloride, Invitrogen, Waltham, MA) with shaking at 37°. *R. torques* was grown anaerobically for two days at 37°C in custom chopped meat broth [13]. The custom chopped meat broth was made as follows: 10g/l beef extract, 30g/l pancreatic digest of casein, 5g/l yeast extract, 5g/l dipotassium phosphate 1mg/l cysteine, 1g/l glucose, 1ml of vitamin K3 (menadione, 1mg/ml stock concentration), 4 ml of hematin/l-histidine solution (1.9mM hematin/0.2M l-histidine stock concentration), 1ml of vitamin B12 (Cyanocobalamin, 0.01mg/ml stock concentration), 10ml of Balch's Vitamins (5mg/l p-aminobenzoic acid, 2mg/l folic acid, 2mg/l biotin, 5mg/l nicotinic acid, 5mg/l calcium pantothenate, 5mg/l riboflavin, 5mg/l thiamine HCl, 10mg/l pyridoxine HCl, 0.1mg/l cyanocobalamin, 5mg/l thioctic acid), 10 ml of Trace Mineral Solution (0.5g/l EDTA, 3g/l magnesium sulfate heptahydrate, 0.5g/l manganese (II) sulfate monohydrate, 1g/l sodium chloride, 0.1g/l iron(II) sulfate heptahydrate, 0.1g/l calcium chloride, 0.1g/l zinc sulfate heptahydrate, 0.01g/l copper (II) sulfate pentahydrate, 0.01g/l boric acid , 0.01g/l sodium molybdate dihydrate, 0.02g/l nickel (II) chloride hexahydrate), 10 ml of Purine/Pyrimidine Solution [adenine, guanine, thymine, cytosine, uracil (all at 200mg/l concentration)] and 10 ml of Amino Acid Solution [alanine, arginine, asparagine, aspartic acid, cysteine, glutamic acid, glutamine, glycine, histidine, isoleucine, leucine, lysine, methionine, phenylalanine, proline, serine, threonine, tryptophan, tyrosine, valine (all at 250mg/l concentration)]. All the reagents were purchased from Sigma, St. Louis, MO, except for the beef extract (BD Difco, Franklin Lakes, NJ).

Intestinal histopathology and disease evaluation—SPF mice were sacrificed at various time points. The cecum and colon were harvested and immediately preserved in freshly made Carnoy's fixative [(anhydrous methanol:chloroform:glacial acetic acid, ratio 60:30:10 v/v, (methanol and chloroform are from Sigma, St. Louis, MO, glacial acetic acid is from Thermo Fisher Scientific, Waltham, MA)] using a protocol described previously with some modifications [51]. The intestinal samples were fixed in Carnoy's solution for 3 h, then transferred to fresh Carnoy's solution for additional 24 h. The samples were then washed in dry methanol and kept at 4 °C until further use. An additional set of mice from

all diet experiments was used to prepare H&E-stained sections. The cecum and colon from this set were flushed with Phosphate buffered saline (PBS, Gibco, Thermo Fisher Scientific, Waltham, MA), fixed in 10% (v/v) formalin (Thermo Fisher Scientific, Waltham, MA) and then processed for H&E staining. Histologic evaluation was performed in a blinded fashion, using a scoring system described previously [13].

Thickness measurements of the colonic mucus layer—Methanol-Carnoy-fixed intestinal samples were embedded in paraffin, cut, and stained with Alcian blue and Alcian blue/PAS (both from Sigma, St. Louis, MO). The staining was performed by the School of Dentistry Histology Core (University of Michigan). The thickness of the colonic inner mucus layer was measured as previously described [22] using partially overlapping photographs, taken from nearly the entire length of each colon based on the Alcian blue stained slides after cross-validation using anti-Muc2 staining. The thickness of the mucus in colonic sections was measured in a blinded fashion using Aperio ImageScope v 12.1.0.5029 (Aperio Technologies, Inc., Leica Microsystems, Wetzlar, Germany). Only regions in which the mucus layer was sandwiched between epithelium on one side and fecal material on the other were used.

Intestinal permeability assay—Intestinal permeability assay was performed using fluorescein isothiocyanate (FITC)-dextran, as described previously [52]. Briefly, mice were deprived of food for 4 h and then gavaged with 0.6 mg/g body weight 4 kDa FITC–dextran (FD4, Sigma-Aldrich St. Louis, MO). Blood was collected 3 h later. The concentration of FITC in serum was determined by spectrophotofluorometry at an excitation of 485 nm and an emission wavelength of 520 nm. FITC-dextran concentrations were determined using a standard curve generated by the serial dilutions of FITC-dextran.

Dextran Sodium Sulfate colitis—Mice were administrated 3% DSS (36–50kDa, MP Biomedicals, Solon, OH) in autoclaved drinking water for 5 days to induce colitis.

ELISA for fecal Lipocalin-2—Frozen fecal samples (−20°C) were used to measure the levels of fecal Lipocalin-2 (Lcn-2) (Duoset murine Lcn-2 ELISA kit, R&D Systems, Minneapolis, MN). Blocking was performed in 1% bovine serum albumin (Thermo Fisher Scientific, Waltham, MA) in PBS, according to manufacturer's instructions. Feces were resuspended in sterile PBS (100 mg/ml), vortexed for 5 min and then centrifuged for 10 min at 13,000 rpm at 4°C. Next, the supernatants were carefully recovered and stored at −20°C until analysis.

Immunofluorescence staining—Slides were deparaffinized twice by submerging in xylene (Thermo Fisher Scientific, Waltham, MA) for five minutes each. The tissue sections were then washed twice in 100% ethanol for five minutes each, followed by rehydration in Milli-Q water for 5 minutes. Antigen retrieval was performed in 10 mM sodium citrate solution (pH 6.0) (Sigma, St. Louis, MO). The submerged sections were heated to 89°C for 10 minutes and then allowed to cool down for 20 minutes at room temperature. Slides were then washed with Milli-Q water and submerged in a blocking buffer [1:10 goat serum (Thermo Fisher Scientific, Waltham, MA) in Tris-buffered Saline (TBS; 500 mM sodium chloride (Sigma, St. Louis, MO), 50 mM Tris (Thermo Fisher Scientific, Waltham, MA),

pH 7.4,] for an hour at room temperature. pH of TBS was adjusted with hydrochloric acid (Thermo Fisher Scientific, Waltham, MA). Sections were then incubated with a 1:80 dilution of Mucin 2 antibody (C3) (GeneTex, Irvine, CA) in a blocking buffer for two hours at room temperature. The slides were rinsed three times in TBS, five minutes each. The secondary antibody staining was performed with a 1:200 dilution of Alexa Fluor 488 conjugated goat anti-rabbit IgG antibody (Thermo Fisher Scientific, Waltham, MA) in a blocking buffer for one hour at room temperature in the dark. Finally, sections were washed twice in TBS for 5 minutes, blotted, and covered with ProLong Gold Antifade reagent with DAPI (Invitrogen, Waltham, MA) and cover slips. The slides were kept overnight at room temperature in the dark, and then kept at 4°C until imaging. The mucus layer in the sections was visualized using an Olympus IX71 inverted fluorescent microscope (Olympus, Center Valley, PA).

Fluorescent In-Situ Hybridization—Methanol-Carnoy-fixed intestinal samples were embedded in paraffin and then cut. FISH was performed on 6μm paraffin-embedded sections as previously described with some modifications [51]. Paraffin sections were dewaxed and washed in 99.5% ethanol. The tissue sections were incubated with 5 μg of Alexa Fluor 555-conjugated EUB (5′-GCTGCCTCCCGTAGGAGT-3′) (bp 337–354 in bacteria EU622773) [51] or a double 3′-and 5′-labelled 16S rRNA targeting probe specific for *Mucispirillum* (Msc487_correct-2xCy3 (CAG TCA CTC CGA ACA ACG CT) [53] in 500 μl of hybridization buffer [20mM Tris-HCl (pH 7.4), 0.1% (w/v) SDS (both from Thermo Fisher Scientific, Waltham, MA), 0.9M NaCl (Sigma, St. Louis, MO)] at 50°C overnight. The sections were rinsed in a wash buffer [20 mM Tris-HCl (pH 7.4), 0.9 M sodium chloride], washed at 50°C for 20 min and counterstained with DAPI (Invitrogen, Waltham, MA). To reduce autofluorescence, the sections were treated with an autofluorescence quenching kit (Vector Laboratories, Burlingame, CA), according to the manufacturer's instruction. Images were recorded using an Olympus IX71 inverted fluorescent microscope (Olympus, Center Valley, PA) within 24 h.

Cecal homogenate preparation—SPF and GF C57BL/6 mice (fed RC or FD for 2 weeks) were euthanized, and the cecum was removed inside an anaerobic chamber (Coy Laboratory Products, Grass Lake, MI). The cecum was opened, contents squeezed into 2 ml of pre-reduced ultrapure water, and the mucus layer was scraped off using coverslips and added to the conical tube. The mixture was then homogenized by vortexing and pipetting, passed through a 0.45μm centrifuge tube filter (Costar, Corning Inc., Corning, NY) to remove large debris, and finally through a 0.22 μm centrifuge tube filter (Costar, Corning Inc., Corning, NY). The resulting cecal homogenates were then dispensed as 200 μl aliquots into a 96-well round bottom plate (Costar, Corning Inc., Corning, NY). *Mucispirillum* was grown on enriched BHI plates for 3 days at 37°C under anaerobic conditions (10% H_2, 5% CO_2 and 85% N_2). *Mucispirillum* was then harvested from the plates with a loop and 1ml of enriched BHI broth, transferred into 4ml of enriched BHI broth and grown anaerobically overnight at 37°C. *E. coli* was grown aerobically in LB broth with shaking overnight at 37°C. For *in vitro* studies, either 5 μl of *E. coli* culture or 10 μl of *Mucispirillum* culture was added to the 96-well round bottom plate (containing the homogenates) and incubated anaerobically at 37°C for up to 3 days. *E. coli* CFUs were enumerated by serial dilution and spot plating on LB plates (LB agar, Invitrogen, Waltham, MA) after 24 h.

Mucispirillum concentration was quantified by qPCR after 3 days. For *ex-vivo* studies, the cecal homogenates were prepared as described above from GF, *E. coli*-, and *R. torques*-monocolonized mice. Once prepared, the cecal homogenates were dispensed as 200 µl aliquots into a 96-well round bottom plate, mixed with 10 µl of *Mucispirillum* culture and incubated anaerobically at 37°C for 3 days. *Mucispirillum* concentration was quantified by qPCR.

Extraction of nucleic acids and quantitative Real-Time PCR—RNA was extracted from both cecal luminal and mucus contents isolated from Tac-DKO mice maintained on RC or FD (for 8 weeks) using a phenol:chloroform:isoamyl alcohol method with bead beating as previously described [22] with a few modifications. Briefly, after the cecal contents and mucus scrapings were freshly harvested, garnet beads (PowerBead tubes, Qiagen, Hilden, Germany) were added to the samples instead of acid-washed glass beads. Next, 500 µl of Buffer A [200 mM NaCl (Sigma, St. Louis, MO), 20 mM EDTA (EDTA solution from Thermo Fisher Scientific, Waltham, MA)], 210 µl of 20% SDS (filter sterilized) (Thermo Fisher Scientific, Waltham, MA) and 500 µl of phenol:chloroform:isoamyl alcohol (125:24:1, pH 4.5; Invitrogen, Waltham, MA) were added to the samples. The mixture was then bead beaten (mini beadbeater, Biospec products, Bartlesville, OK) for 2 min and centrifuged at 4 °C (3 min at 13000 rpm). The aqueous phase was recovered and mixed with 500 µl of the aforementioned phenol:chloroform:isoamyl alcohol solution. Afterwards, the mixture was centrifuged at 4°C (3 min at 13,000 rpm) and the aqueous phase was recovered. 1/10 volume of the 3M sodium acetate solution (pH: 5.2, Sigma, St. Louis, MO) and 1 volume of −20°C chilled 100% ethanol (Thermo Fisher Scientific, Waltham, MA) were added to the aqueous phase. The resulting solution was then mixed by inversion and incubated for 20 min on ice. Afterwards, the mixture was centrifuged at 4°C for 20 min at 13,000 rpm. The pellet was recovered and washed in 500 µl of cold 70% ethanol. The mixture was centrifuged at 4°C (5 min at 13,000 rpm) and the RNA pellet was recovered, air dried and then resuspended in 100µl nuclease-free water. The RNA extracts were then further purified using an RNeasy Mini kit (Qiagen, Hilden, Germany) for luminal contents and an Rneasy Micro kit (Qiagen, Hilden, Germany) for mucus samples. 10µl of 2-Mercaptoethanol (Sigma, St. Louis, MO) was added to the provided extraction buffer according to the manufacturer's protocol. Total RNA was submitted to the Advanced Genomics Core at the University of Michigan for sequencing.

RNA was extracted from colonic tissue using the E.Z.N.A. Total RNA Kit (Omega Biotek, Norcross, GA) according to the manufacturer's instructions. RNA was reverse transcribed using the High Capacity RNA-to-cDNA Kit (Applied Biosystems, Waltham, MA) and the resulting cDNA was utilized for quantitative real time RT-PCR (qPCR). Genomic DNA was extracted from fecal pellets using the E.Z.N.A stool DNA kit (Omega Bio-Tek, Norcross, GA) according to the manufacturer's protocol. Genomic DNA was extracted from colonic mucus scrapings using the E.Z.N.A stool DNA kit (Omega Bio-Tek, Norcross, GA) following incubation with 1mg lysozyme (Sigma, St. Louis, MO) for 15 min at room temperature. DNA was then used for qPCR.

qPCR was performed using a SYBR green PCR master mix (Alkali Scientific, Fort Lauderdale, FL) and StepOne Real-time PCR system (Applied Biosystems, Waltham, MA).

The primer sequences used for the detection of each gene were summarized separately (Table S7) [13,54–59]. Relative mRNA expression was calculated by the ΔΔCt method and normalized to the expression of either GAPDH or to the universal 16S rRNA gene (for *in vivo* studies). Analysis was performed in duplicate sample sets. Specificity of each primer was validated by the following approaches: 1) by qPCR against target species genome and melting curve analysis (for a single peak), 2) by qPCR for each primer set against a non-target template. Genomic DNA of *Mucispirillum* and *R. torques* were used to generate standard curves to determine target concentrations (for *in vitro* studies). Copy numbers of host DNA and bacterial 16S rRNA gene sequences were determined by comparison with known quantities of mouse and *E. coli* genomic DNA. Bacterial genome copies were estimated by qPCR using universal v4 16S rRNA primers and normalized by total DNA. Host genomic copy numbers were determined by qPCR using *ACTB* primers and normalized by total DNA.

Microbiota analyses—For the 16S rRNA sequencing, PCR and library preparation were performed by the Microbiome Core by the University of Michigan. Amplicons of the V4 region within the 16S rRNA gene were generated and both ends of the fragments were sequenced using an Illumina MiSeq instrument. The paired end sequences were curated using Mothur (v.1.40.5) as previously described [60,61]. Briefly, the paired end sequences were assembled into ≈ 250 bp contigs, aligned to the SILVA 16S rRNA database release 138[62], made free of possible chimeric sequences by UCHIME[63], binned into Operational taxonomic units (OTUs) at >97 % identity level and taxonomically assigned with 16S rRNA gene training set version 16 of Ribosomal Database Project. α-diversity (Shannon index) and NMDS plot of β-diversity values, LEfSe Linear discriminant analysis (LDA) values of OTUs were all determined using Mothur. To identify significant differentially abundant OTUs, bacterial taxa were screened with pairwise LEfSe analysis, and further verified by multiple hypothesis testing using the false discovery rate (FDR) of signal-to-noise ratio with Morpheus (https://software.broadinstitute.org/morpheus/, permutations=9999, markers=0). Heat maps of OTUs were visualized by MeV. To label individual OTUs, we chose the lowest taxa that were not identified as “unclassified”. All the samples that had zero *Mucispirillum* reads during all time points of the dietary interventions were removed. The phylogenetic tree was calculated by Phylogeny.fr [64] using the most abundant sequences of indicated OTUs that were extracted by Mothur and sort/uniq Linux commands. *R. torques* VIII-239, derived from PRJNA227979, was included in the phylogenetic analysis. The figure (Figure S5A) was drawn by TreeGraph2.

Microbial RNA-Sequencing analysis—Library preparation and sequencing of the RNA-seq libraries were performed by the Advanced Genomics Core at the University of Michigan. Briefly, RNA was assessed for quality using the TapeStation (Agilent, Santa Clara, CA). Samples were prepared using the New England BioLabs (NEB)Next Ultra II Directional RNA Library Prep Kit for Illumina, the Ribo depletion Module NEBNext rRNA (Human/Mouse/Rat), the NEBNext rRNA Depletion Kit (Bacteria), and the NEBNext Multiplex Oligos for Illumina Unique dual (all from NEB, Ipswitch, MA) where 115ng of total RNA was ribosomal depleted using the rRNA Depletion modules. The rRNA-depleted RNA is then fragmented 15 minutes determined by RIN (RNA Integrity Number) of input

RNA as per protocol and copied into first strand cDNA using reverse transcriptase and dUTP mix. Samples underwent end repair and dA-Tailing step, followed by ligation of NEBNext adapters. The products were purified and enriched by 13 cycles of PCR to create the final cDNA library, which were checked for quality and quantity by Qubit hsDNA (Thermo Fisher Scientific, Waltham, MA) and LabChip (PerkinElmer, Waltham, MA). The samples were pooled and sequenced on the Illumina NovaSeq S4 Paired-end 150bp, according to manufacturer's recommended protocols (Illumina, San Diego, CA). bcl2fastq2 Conversion Software (Illumina) was used to generate de-multiplexed Fastq files. Contaminated host sequences were removed by Bowtie2 [65].

Analysis of *Mucispirillum* gene transcripts—The transcript levels of individual genes in *Mucispirillum schaedleri* ASF457 (GCA_000487995) were mapped, counted and annotated by Salmon [66]. For a more detailed annotation, closest protein sequences and species were identified by Diamond using Uniref100 of UniProt database (https://www.uniprot.org/).

Analysis of hydrogenase transcripts—To identify hydrogenase transcripts and metagenome-assembled genomes (MAGs), core sequences with homology were obtained by Diamond (e-value < 10^{-5}) [67] from either mouse (mucus and luminal) or human pediatric (stool) IBD sequences (SRP057027,[26] respectively, and assembled by metaSPAdes [68]. Finally, pooled sequences were verified by Diamond using reference sequences downloaded from HydDB database [69] Transcript reads were further obtained by four-time repetitive expansion of transcript sizes (detected by Bowtie2) and *de novo* assembly by metaSPAdes. Metagenomic reads were directly counted after removing low read samples (<5000 target reads). For putative H_2-generating hydrogenases, we used all HydDB reference sequences from NiFe group 4a and FeFe groups A1 and B. Hydrogenases (from FeFe groups A1 and B) were further screened by two criteria, >70 % identity to the references and higher homology to FeFe group A1/B rather than non-A1/B FeFe hydrogenases. For a more detailed annotation, closest protein sequences and species were identified by Diamond using Uniref100 of UniProt database. Microbial species that were identical to Lachnospiraceae unclassified, Lachnospiraceae [*Ruminococcus*] (not Ruminococcaceae *Ruminococcus*), and the species with higher homology (but not identical) to Lachnospiraceae spp. were classified as Lachnospiraceae spp (Figure 6B). The reads were counted by Salmon and a pairwise comparison of TPM (individual transcript per million of hydrogenases) was performed by the "marker selection" function of Morpheus (https://software.broadinstitute.org/morpheus/). Log_{10}[TPM] values were assigned (visualized by MeV), 1/2 being the minimal TPM, to all transcripts as the detection threshold for error suppression of log calculation.

Bacterial growth assays in a custom carbohydrate array—The custom carbohydrate array was formulated and performed as previously described [22]. The carbon sources (all at 10mg/ml, except those specified below) included in the array were: arabinose, fructose, fucose, galactose, galacturonic acid, glucosamine, glucose, glucuronic acid, mannose, N-acetylgalactosamine, N-acetylglucosamine, N-acetylneuraminic acid (IV-S), rhamnose, ribose, xylose, inulin (chicory), amylopectin (maize), amylopectin (potato), cellobiose, chondroitin sulfate, heparin hyaluronan, glycogen mannan (*S. cerevisiae*),

laminarin, alginate (brown algae), dextran (*L. mesenteroides*), levan (*E. herbicola*), pullulan (*A. pullulans*) (all from Sigma, St. Louis, MO), arabinan (sugar beet), arabinogalactan (larch), pectic galactan (potato), pectic galactan (lupin), rhamnogalacturonan I (potato pectin) (20mg/ml), arabinoxylan (wheat), β-glucan (barley), galactomannan (carob), glucomannan (koniac), xyloglucan (tamarind), lichenan (all from Megazyme-Neogen, Lansing, MI) fructooligosaccharides (commercial food supply), mucin *O*-glycans [provided by Dr. E.C. Martens, (20mg/ml)]. Additional carbon sources, such as acid casein peptone (1% and 10% w/v) and glycerol (1% and 10% v/v) (both from Thermo Fisher Scientific, Waltham, MA) were tested. Growth assays for all carbohydrates were carried out in non-adjacent duplicates and contained two non-adjacent water only samples (negative controls) and two non-adjacent enriched BHI (with glucose and serum) samples (positive controls). *Mucispirillum* was grown on enriched BHI plates for 3 days at 37°C under anaerobic conditions (10% H_2, 5% CO_2 and 85% N_2). *Mucispirillum* was then harvested from the plates with a loop and 1ml of enriched BHI broth, transferred into 4ml of enriched BHI broth and grown anaerobically overnight at 37°C. *E.coli* was grown aerobically overnight at 37°C in LB broth with shaking. For growth profiling in a custom carbohydrate array, 1 ml of each culture was anaerobically centrifugated. The pellet was recovered and washed 2 times in 2x concentrated BHI medium without any carbohydrates and serum for *Mucispirillum*, and 2x concentrated carbohydrate-free minimal medium (M9 with the addition of 4mM magnesium sulfate, 200μM calcium chloride, 2μM ferrous sulfate, all from Sigma, St. Louis, MO) for *E.coli* to remove carried over carbohydrates from the culture media. The pellets were finally resuspended in 1 ml of 2x concentrated BHI broth and M9 minimal medium without any carbohydrates and serum, respectively. This 1 ml culture was used to inoculate 50 ml of 2x concentrated medium (either BHI broth or M9 minimal medium without carbohydrates and serum) at a 1:50 ratio, respectively. 100 μl of the resulting cultures were then added to the individual wells of the carbohydrate solutions in the 96-well plates, resulting in 200 μl of final volume.

Absorbance values were measured at 600 nm (A600) at an interval of 10 min over 72 h. To construct a heat map containing relative growth values (Figure 4A), absorbance data of all bacterial species were normalized as follows: only carbohydrate growth assays for which both replicate cultures produced an increase in absorbance of more than 0.1 were scored as positive (all other values were set to 0), the starting absorbance on each substrate was subtracted. Next, the maximum change in absorbance was normalized within each individual species by setting its best growth to 1.0 and normalizing all other positive growths to this maximum value (normalized values were thus between 0 and 1.0). Both raw and normalized values are provided in Table S2. Each positive growth curve was manually inspected to validate the presence of an exponential growth profile.

Additionally, 50 μl of the 1 ml *Mucispirillum* culture (resuspended in BHI medium without carbohydrates and serum) were used to inoculate 5 ml of BHI medium (without carbohydrates and serum) in the presence of either acid casein peptone or glycerol and grown in borosilicate glass culture tubes (Thermo Fisher Scientific, Waltham, MA) for three days. *Mucispirillum* growth was then analyzed by qPCR. BHI medium only (negative) and carbohydrate-free BHI medium with serum (positive) were included as controls.

Purification of porcine colonic mucin oligosaccharides and bacterial growth— Highly sulfated porcine colonic mucin oligosaccharides (referred as rectal glycoproteins, rGP) were purified from the distal porcine colon and rectum using a protocol described previously [70]. Briefly, distal porcine colon and rectum were opened, and the fecal contents were removed. The mucosa was scraped off, and mucus was extracted by homogenizing the tissue in at least 5 volumes of extraction buffer (6 M guanidine chloride, 5 mM EDTA, 10 mM sodium phosphate monobasic, pH 6.5, all from Sigma, St. Louis, MO). The samples were gently stirred at 4 °C for 16 h. The solution was then spun down at 15,000 r.p.m. for 30 min at 10 °C, and the supernatant was discarded. Pellets were resuspended in the extraction buffer, and the process was repeated until the supernatant was clear for at least two extractions. After extraction, the mucins were solubilized by disulfide bonds reduction. Pellets were resuspended in the fresh reduction buffer [6 M guanidine chloride, 5 mM EDTA (both from Sigma, St. Louis, MO), 0.1 M Tris (Thermo Fisher Scientific, Waltham, MA) pH 8.0] containing 25 mM of 1,4-dithiothreitol (DL-Dithiothreitol from Sigma, St. Louis, MO) and slowly stirred at 37 °C for 5 h. After this incubation, 62.5 mM iodoacetamide (Sigma, St. Louis, MO) was added and the solution was stirred slowly in the dark at room temperature for 16 h. The solution was then centrifuged at 10,000 r.p.m. at 4 °C for 30 min, and the supernatant containing the solubilized mucins was extensively dialysed into water. Samples were dissolved into 100 mM Tris-HCl, pH 8.0 (Thermo Fisher Scientific, Waltham, MA), containing 1 mg ml–1 trypsin (Sigma-Aldrich, St. Louis, MO), and incubated with slow stirring at 37 °C for 16 h. Additionally, after trypsin treatment the sample was dialyzed against water and lyophilized. Finally, rGP solution (5 mg/ml concentration in PBS) was autoclaved for 5 minutes (sterilization cycle). 100 µl of rGP (5 mg/ml concentration in PBS), glucose (10 mg/ml concentration, sterile filtered in water) and rhamnose (10 mg/ml concentration, sterile filtered in water) solutions were added to flat bottom 96-well plates (Costar, Corning Inc., Corning, NY). The plates were then transferred to an anaerobic chamber (Coy Laboratory Products, Grass Lake, MI) and allowed to equilibrate in the anaerobic atmosphere for ~3–4 h. Growth assays were carried out in triplicates and contained three medium only samples (negative controls). *Mucispirillum* was grown on enriched BHI plates for 3 days at 37°C under anaerobic conditions. *Mucispirillum* was then recovered from the plates with a loop and 1 ml of enriched BHI broth, transferred into 5ml of enriched BHI broth and grown anaerobically overnight at 37°C. *R. torques* was grown in pre-reduced custom chopped meat broth for 2 days at 37°C under anaerobic conditions. For growth profiling in the presence of rGP, glucose and rhamnose, 1 ml of each culture was anaerobically centrifugated. The pellet was recovered and washed 2 times in 2x concentrated chopped meat broth without any carbohydrates to remove carried over carbohydrates from the culture media. The pellet was then resuspended in 1 ml of 2x concentrated chopped meat broth without any carbohydrates. This 1 ml culture was used to inoculate 50 ml of 2x concentrated chopped meat broth without any carbohydrates at a 1:50 ratio. 100 µl (for single *R. torques or Mucispirillum* cultures) or 50 µl (for *R. torques* and *Mucispirillum* co-cultures) of the resulting cultures were then added to the individual wells of the rGP, glucose and rhamnose solutions in the 96-well plates, resulting in 200 µl final volumes. The absorbance measurements were performed as described above, and bacterial growth was quantified by qPCR.

Bacterial oral challenge—For *in vivo* inoculations, *Mucispirillum* was grown anaerobically on enriched BHI plates. A ratio of one plate/mouse was used for *in vivo* experiments. Three-week-old (both male and female) Jax DKO mice were co-housed as appropriate for gender, right after weaning, for 5 weeks. Jax-DKO mice were then randomly assigned to groups and fed either the RC or the FD diet (for the duration of the experiment). One week later, the animals were treated with vancomycin (250 mg/l in drinking water, Xellia Pharmaceuticals, Buffalo Grove, IL) for 7 days and finally switched to regular water. Among antibiotics usually used to deplete microbiota in SPF, vancomycin is one that mainly targets Gram-positive microbe, and it was used as it doesn't not affect colonization of Gram-negative *Mucispirillum* and rather enhances it in SPF mice (based on our preliminary experiments). Mice were then colonized (oral gavage) with 0.2 ml of BHI broth containing approximately 1×10^8 CFU of *Mucispirillum* every other day for 7 days. Mouse survival and body weights were monitored for 7 days after the first oral administration. RC-fed male and female littermate *Muc2*$^{-/-}$ and *Muc2*$^{+/-}$ mice were separated at five-week of age (after 2 weeks of cohousing), then treated with vancomycin (250 mg/l in drinking water) for 7 days and finally switched to regular water. Mice were then infected (oral gavage) with 0.2 ml of BHI broth containing approximately 1×10^8 CFU of *Mucispirillum* and sacrificed one day after bacterial administration. To determine bacterial loads and to monitor the development of intestinal inflammation, fecal samples were collected before and every other day for 7 days in Jax-DKO mice, and until day 1 in *Muc2*$^{-/-}$ and *Muc2*$^{+/-}$ mice, following the first bacterial administration. The abundance of *Mucispirillum* was quantified by qPCR and level of intestinal inflammation was determined using lipocalin-2 ELISA. Jax-DKO mice were sacrificed 7 days after the first infection, while *Muc2*$^{-/-}$ and *Muc2*$^{+/-}$ mice were sacrificed on day 1. Cecum and colon tissue was harvested and processed for mucus thickness measurement and histological examination.

GF C57BL/6 mice were inoculated with either *E. coli* K12 BW25113 or *R. torques VIII* (0.2 ml of bacterial suspension/mouse, ~10^9 CFU). Mono-colonization with either *E.coli* or *R. torques* was confirmed by qPCR. Mono-colonization with *R. torques VIII* was achieved by treatment with 100mM succinate (disodium succinate, Sigma, St. Louis, MO) for 7 days prior the bacterial gavage, a strategy which is used to reduce the oxygen concentration in the gut of GF mice and allow colonization with strict anaerobes [71]. Succinate treatment was administrated only to *R. torques* group and stopped two weeks prior *Mucispirillum* administration to avoid it could have affected it. For *ex-vivo* studies, GF, *E. coli*- and *R. torques*-monocolonized mice were euthanized 2 weeks after reconstitution and used to prepared cecal homogenates (see above). For *in vivo* studies, GF, *E. coli*- and *R. torques* monocolonized C57BL/6 mice (2 weeks after reconstitution) received 0.2 ml of BHI broth (oral gavage) containing approximately 1×10^8 CFU of *Mucispirillum.* To determine bacterial loads, fecal samples were collected before and every week for up to 2 weeks following *Mucispirillum* administration. The abundance of *Mucispirillum* was quantified by qPCR. In additional *in vivo* experiments, GF and *R. torques* monocolonized C57BL/6 mice were sacrificed 2 weeks after reconstitution. Large intestine was harvested, and the mucus thickness was assessed as described above.

Bacterial co-culture in absence/presence of exogenous H_2—Culture medium tubes were prepared by adding 5 ml nitrate-supplemented enriched BHI [(BHI with 10mM sodium nitrate (Sigma, St. Louis, MO)] to sterilized Balch tubes that were subsequently sealed with sterilized butyl rubber stoppers. The culture medium (nitrate-supplemented BHI) was then rendered anaerobic by the vacuum-vortex technique of Wolfe and Metcalf [72] with six cycles, using a mixture of either 80% N_2-20% CO_2 or 80% H_2-20% CO_2 (Cryogenic Gases, Detroit, MI). Medium tubes were incubated in a water bath at 50°C until the resazurin indicator (Sigma, St. Louis, MO) was observed to become colorless. Medium tubes were inoculated with 50ul of *Mucispirillum* starter culture in the presence of absence of *R. torques* (50ul starter culture) and incubated with shaking at 37°C for 3 days. *Mucispirillum* and *R. torques* concentrations were quantified by qPCR.

Bioreactors—Co-cultures of *R. torques* and *Mucispirillum* species were grown in bioreactor vessels (Wyse Glass, Midland, MI) operated in batch mode. The bioreactors were filled with 150 ml of nitrate-supplemented enriched BHI and inoculated with 1.5 ml each of *R. torques* and *Mucispirillum* species starter cultures. The cultures were kept at 37°C using a recirculating water jacket, stirred, and sparged with a mixed gas containing 20% CO_2 and either 80% N_2 (Cryogenic Gases, Detroit, MI) or 80% H_2 (Cryogenic Gases, Detroit, MI) for 3 days. *Mucispirillum* concentration was quantified by qPCR.

H_2 measurements—Dissolved H_2 was quantified using a method derived from Kraemer and Bagley [40]. Samples of 0.5 mL culture liquid were immediately added to 1 ml 3M sulfuric acid (Sigma, St. Louis, MO) in sealed Hungate tubes. The tubes were vortexed vigorously and incubated for >2 hrs at room temperature to extract dissolved H_2 into the gas phase. The pressure in the tube headspaces was then adjusted to 10 psig with pure N_2 and 2 ml samples were withdrawn for analysis of H_2 content.

H_2 content was measured using a Peak Performer 1 gas chromatograph (Cat#910-105) with a reducing compound photometer (RCP) detector and post-column diluter (Peak Laboratories, Mountain View, CA) calibrated using a 10 ppm H_2 standard (GASCO 105L-H2N-10, Cal Gas Direct Incorporate, Huntington Beach, CA). Ultra-high purity N_2 was used as the carrier gas.

To quantify H_2 in culture headspaces, 0.5 ml of headspace gas was transferred from each culture into a sealed Balch tube containing air. 10 ml of air was then added to each tube to facilitate sample withdrawal and pumped in and out several times to mix the gases. 2 ml samples were withdrawn from the Balch tubes, further diluted using syringes fitted with stopcocks if necessary, and analyzed for H_2 content using the Peak Performer 1 gas chromatograph (Peak Laboratories, Mountain View, CA).

Ammonia assay—The concentration of ammonium in culture supernatants was measured in triplicates using a Synergy H1 Multi-Mode Microplate Reader (BioTek Instruments, Winooski, VT) using Gen5™ software (BioTek Instruments, Winooski, VT) following the manual phenol hypochlorite method (detection limit 1μg N l^{-1}) [73]. Briefly, 500μl of culture supernatant was mixed with 20ul of phenol solution [(11% w/vol phenol (Thermo Fisher Scientific, Waltham, MA) dissolved in ethanol)]. Next, 20 μl of sodium nitroprusside

solution [(0.5% w/vol sodium nitroprusside (Fisher Scientific, Waltham, MA) dissolved in distilled deionized water)] was added to the mixture and the solution was thoroughly mixed. Then 50 µl of oxidizing solution [(16% w/vol sodium citrate (Thermo Fisher Scientific, Waltham, MA), 0.8% w/vol sodium hydroxide (Thermo Fisher Scientific, Waltham, MA), and 4% sodium hypochlorite dissolved in distilled deionized water] was added and mixed thoroughly. The mixture was incubated for 4 h at room temperature, then 200 µl of the mixture was transferred to an assay plate and absorbance was measured at 640 nm. Ammonia/ammonium concentration was determined according to a standard curve [prepared using ammonium chloride (Fisher Scientific, Waltham, MA)].

Quantification and Statistical analysis—Unless otherwise stated in individual method sections above, all statistical analyses were performed using Prism 9.1.0 (GraphPad Software, San Diego, CA). Sample sizes were chosen to reach statistical significance ($p < 0.05$) for a pre-determined effect based on the sample variation observed in previous studies. Sample sizes for microbiota analysis were chosen based on sample sizes published in previous studies. Differences between two groups were evaluated using two-tailed unpaired t-test (parametric) or Mann–Whitney U test (nonparametric). Comparisons of more than two groups were performed with one-way ANOVA (parametric) or two-way repeated measures ANOVA (parametric) or Kruskal–Wallis test (non-parametric) followed by Tukey's, Sidak's or Dunn's multiple comparisons test. Differences of $p < 0.05$ were considered significant in all statistical analyses. Numbers of animals (n) used in individual experiments, details of the statistical tests used and pooled values for several biological replicates are indicated in the respective figure legends.

Supplementary Material

Refer to Web version on PubMed Central for supplementary material.

ACKNOWLEDGMENTS

The authors thank Kelsey Martin and Amr Aboud for animal husbandry, Jani L. O'Rourke for bacterial strain, Grace Chen for critical reading of the manuscript, Nicholas A. Pudlo for technical assistance, and the Microbiome Core, the Germ-Free Mouse Facility, the Advanced Genomics Core, the School of Dentistry Histology Core, the Digital Pathology (Slide Scanning service) at the University of Michigan for support. This work was supported by Senior Research Award from the Crohn's and Colitis Foundation (1005572) (R.C), Pilot Feasibility Project through the University of Michigan Center for Gastrointestinal Research (NIH P30 DK034933) (R.C.), and NIH grant 5R01 DK121504 (G.N.).

INCLUSION AND DIVERSITY

We support inclusive, diverse, and equitable conduct of research.

REFERENCES

1. Xavier RJ, and Podolsky DK (2007). Unravelling the pathogenesis of inflammatory bowel disease. Nature 448, 427–434. 10.1038/nature06005. [PubMed: 17653185]
2. Peloquin JM, Goel G, Villablanca EJ, and Xavier RJ (2016). Mechanisms of Pediatric Inflammatory Bowel Disease. Annu Rev Immunol 34, 31–64. 10.1146/annurev-immunol-032414-112151. [PubMed: 27168239]

3. Ng SC, Shi HY, Hamidi N, Underwood FE, Tang W, Benchimol EI, Panaccione R, Ghosh S, Wu JCY, Chan FKL, et al. (2017). Worldwide incidence and prevalence of inflammatory bowel disease in the 21st century: a systematic review of population-based studies. Lancet 390, 2769–2778. 10.1016/S0140-6736(17)32448-0. [PubMed: 29050646]
4. Windsor JW, and Kaplan GG (2019). Evolving Epidemiology of IBD. Curr Gastroenterol Rep 21, 40. 10.1007/s11894-019-0705-6. [PubMed: 31338613]
5. Benchimol EI, Mack DR, Nguyen GC, Snapper SB, Li W, Mojaverian N, Quach P, and Muise AM (2014). Incidence, outcomes, and health services burden of very early onset inflammatory bowel disease. Gastroenterology 147, 803–813 e807; quiz e814–805. 10.1053/j.gastro.2014.06.023. [PubMed: 24951840]
6. Benchimol EI, Fortinsky KJ, Gozdyra P, Van den Heuvel M, Van Limbergen J, and Griffiths AM (2011). Epidemiology of pediatric inflammatory bowel disease: a systematic review of international trends. Inflamm Bowel Dis 17, 423–439. 10.1002/ibd.21349. [PubMed: 20564651]
7. Caruso R, Lo BC, and Nunez G (2020). Host-microbiota interactions in inflammatory bowel disease. Nat Rev Immunol 20, 411–426. 10.1038/s41577-019-0268-7. [PubMed: 32005980]
8. McGovern DP, Kugathasan S, and Cho JH (2015). Genetics of Inflammatory Bowel Diseases. Gastroenterology 149, 1163–1176 e1162. 10.1053/j.gastro.2015.08.001. [PubMed: 26255561]
9. Liu JZ, van Sommeren S, Huang H, Ng SC, Alberts R, Takahashi A, Ripke S, Lee JC, Jostins L, Shah T, et al. (2015). Association analyses identify 38 susceptibility loci for inflammatory bowel disease and highlight shared genetic risk across populations. Nat Genet 47, 979–986. 10.1038/ng.3359. [PubMed: 26192919]
10. Ananthakrishnan AN, Huang H, Nguyen DD, Sauk J, Yajnik V, and Xavier RJ (2014). Differential effect of genetic burden on disease phenotypes in Crohn's disease and ulcerative colitis: analysis of a North American cohort. Am J Gastroenterol 109, 395–400. 10.1038/ajg.2013.464. [PubMed: 24419484]
11. Li Q, Lee CH, Peters LA, Mastropaolo LA, Thoeni C, Elkadri A, Schwerd T, Zhu J, Zhang B, Zhao Y, et al. (2016). Variants in TRIM22 That Affect NOD2 Signaling Are Associated With Very-Early-Onset Inflammatory Bowel Disease. Gastroenterology 150, 1196–1207. 10.1053/j.gastro.2016.01.031. [PubMed: 26836588]
12. Muise AM, Xu W, Guo CH, Walters TD, Wolters VM, Fattouh R, Lam GY, Hu P, Murchie R, Sherlock M, et al. (2012). NADPH oxidase complex and IBD candidate gene studies: identification of a rare variant in NCF2 that results in reduced binding to RAC2. Gut 61, 1028–1035. 10.1136/gutjnl-2011-300078. [PubMed: 21900546]
13. Caruso R, Mathes T, Martens EC, Kamada N, Nusrat A, Inohara N, and Nunez G (2019). A specific gene-microbe interaction drives the development of Crohn's disease-like colitis in mice. Sci Immunol 4. 10.1126/sciimmunol.aaw4341.
14. Gevers D, Kugathasan S, Denson LA, Vazquez-Baeza Y, Van Treuren W, Ren B, Schwager E, Knights D, Song SJ, Yassour M, et al. (2014). The treatment-naive microbiome in new-onset Crohn's disease. Cell Host Microbe 15, 382–392. 10.1016/j.chom.2014.02.005. [PubMed: 24629344]
15. Cipcic Paljetak H, Baresic A, Panek M, Peric M, Matijasic M, Lojkic I, Barisic A, Vranesic Bender D, Ljubas Kelecic D, Brinar M, et al. (2022). Gut microbiota in mucosa and feces of newly diagnosed, treatment-naive adult inflammatory bowel disease and irritable bowel syndrome patients. Gut Microbes 14, 2083419. 10.1080/19490976.2022.2083419. [PubMed: 35695669]
16. Limketkai BN, Shah ND, Sheikh GN, and Allen K (2019). Classifying Enteral Nutrition: Tailored for Clinical Practice. Curr Gastroenterol Rep 21, 47. 10.1007/s11894-019-0708-3. [PubMed: 31368086]
17. Logan M, Gkikas K, Svolos V, Nichols B, Milling S, Gaya DR, Seenan JP, Macdonald J, Hansen R, Ijaz UZ, et al. (2020). Analysis of 61 exclusive enteral nutrition formulas used in the management of active Crohn's disease-new insights into dietary disease triggers. Aliment Pharmacol Ther 51, 935–947. 10.1111/apt.15695. [PubMed: 32249975]
18. van Rheenen PF, Aloi M, Assa A, Bronsky J, Escher JC, Fagerberg UL, Gasparetto M, Gerasimidis K, Griffiths A, Henderson P, et al. (2020). The Medical Management of Paediatric Crohn's Disease: an ECCO-ESPGHAN Guideline Update. J Crohns Colitis. 10.1093/ecco-jcc/jjaa161.

19. Lee D, Baldassano RN, Otley AR, Albenberg L, Griffiths AM, Compher C, Chen EZ, Li H, Gilroy E, Nessel L, et al. (2015). Comparative Effectiveness of Nutritional and Biological Therapy in North American Children with Active Crohn's Disease. Inflamm Bowel Dis 21, 1786–1793. 10.1097/MIB.0000000000000426. [PubMed: 25970545]
20. Cohen-Dolev N, Sladek M, Hussey S, Turner D, Veres G, Koletzko S, Martin de Carpi J, Staiano A, Shaoul R, Lionetti P, et al. (2018). Differences in Outcomes Over Time With Exclusive Enteral Nutrition Compared With Steroids in Children With Mild to Moderate Crohn's Disease: Results From the GROWTH CD Study. J Crohns Colitis 12, 306–312. 10.1093/ecco-jcc/jjx150. [PubMed: 29165666]
21. Damas OM, Garces L, and Abreu MT (2019). Diet as Adjunctive Treatment for Inflammatory Bowel Disease: Review and Update of the Latest Literature. Curr Treat Options Gastroenterol 17, 313–325. 10.1007/s11938-019-00231-8. [PubMed: 30968340]
22. Desai MS, Seekatz AM, Koropatkin NM, Kamada N, Hickey CA, Wolter M, Pudlo NA, Kitamoto S, Terrapon N, Muller A, et al. (2016). A Dietary Fiber-Deprived Gut Microbiota Degrades the Colonic Mucus Barrier and Enhances Pathogen Susceptibility. Cell 167, 1339–1353 e1321. 10.1016/j.cell.2016.10.043. [PubMed: 27863247]
23. Earle KA, Billings G, Sigal M, Lichtman JS, Hansson GC, Elias JE, Amieva MR, Huang KC, and Sonnenburg JL (2015). Quantitative Imaging of Gut Microbiota Spatial Organization. Cell Host Microbe 18, 478–488. 10.1016/j.chom.2015.09.002. [PubMed: 26439864]
24. Schroeder BO, Birchenough GMH, Stahlman M, Arike L, Johansson MEV, Hansson GC, and Backhed F (2018). Bifidobacteria or Fiber Protects against Diet-Induced Microbiota-Mediated Colonic Mucus Deterioration. Cell Host Microbe 23, 27–40 e27. 10.1016/j.chom.2017.11.004. [PubMed: 29276171]
25. Lee D, Albenberg L, Compher C, Baldassano R, Piccoli D, Lewis JD, and Wu GD (2015). Diet in the pathogenesis and treatment of inflammatory bowel diseases. Gastroenterology 148, 1087–1106. 10.1053/j.gastro.2015.01.007. [PubMed: 25597840]
26. Lewis JD, Chen EZ, Baldassano RN, Otley AR, Griffiths AM, Lee D, Bittinger K, Bailey A, Friedman ES, Hoffmann C, et al. (2015). Inflammation, Antibiotics, and Diet as Environmental Stressors of the Gut Microbiome in Pediatric Crohn's Disease. Cell Host Microbe 18, 489–500. 10.1016/j.chom.2015.09.008. [PubMed: 26468751]
27. Chassaing B, Srinivasan G, Delgado MA, Young AN, Gewirtz AT, and Vijay-Kumar M (2012). Fecal lipocalin 2, a sensitive and broadly dynamic non-invasive biomarker for intestinal inflammation. PLoS One 7, e44328. 10.1371/journal.pone.0044328. [PubMed: 22957064]
28. Conrad MA, Carreon CK, Dawany N, Russo P, and Kelsen JR (2019). Distinct Histopathological Features at Diagnosis of Very Early Onset Inflammatory Bowel Disease. J Crohns Colitis 13, 615–625. 10.1093/ecco-jcc/jjy212. [PubMed: 30551128]
29. Parrish A, Boudaud M, Grant ET, Willieme S, Neumann M, Wolter M, Craig SZ, De Sciscio A, Cosma A, Hunewald O, et al. (2023). Akkermansia muciniphila exacerbates food allergy in fibre-deprived mice. Nat Microbiol. 10.1038/s41564-023-01464-1.
30. Aihara E, Engevik KA, and Montrose MH (2017). Trefoil Factor Peptides and Gastrointestinal Function. Annu Rev Physiol 79, 357–380. 10.1146/annurev-physiol-021115-105447. [PubMed: 27992733]
31. Robertson BR, O'Rourke JL, Neilan BA, Vandamme P, On SLW, Fox JG, and Lee A (2005). Mucispirillum schaedleri gen. nov., sp. nov., a spiral-shaped bacterium colonizing the mucus layer of the gastrointestinal tract of laboratory rodents. Int J Syst Evol Microbiol 55, 1199–1204. 10.1099/ijs.0.63472-0. [PubMed: 15879255]
32. Petersson J, Schreiber O, Hansson GC, Gendler SJ, Velcich A, Lundberg JO, Roos S, Holm L, and Phillipson M (2011). Importance and regulation of the colonic mucus barrier in a mouse model of colitis. Am J Physiol Gastrointest Liver Physiol 300, G327–333. 10.1152/ajpgi.00422.2010. [PubMed: 21109593]
33. Johansson ME, Phillipson M, Petersson J, Velcich A, Holm L, and Hansson GC (2008). The inner of the two Muc2 mucin-dependent mucus layers in colon is devoid of bacteria. Proc Natl Acad Sci U S A 105, 15064–15069. 10.1073/pnas.0803124105. [PubMed: 18806221]

34. Vacca M, Celano G, Calabrese FM, Portincasa P, Gobbetti M, and De Angelis M (2020). The Controversial Role of Human Gut Lachnospiraceae. Microorganisms 8. 10.3390/microorganisms8040573.
35. Png CW, Linden SK, Gilshenan KS, Zoetendal EG, McSweeney CS, Sly LI, McGuckin MA, and Florin TH (2010). Mucolytic bacteria with increased prevalence in IBD mucosa augment in vitro utilization of mucin by other bacteria. Am J Gastroenterol 105, 2420–2428. 10.1038/ajg.2010.281. [PubMed: 20648002]
36. Zumft WG (1997). Cell biology and molecular basis of denitrification. Microbiol Mol Biol Rev 61, 533–616. 10.1128/mmbr.61.4.533-616.1997. [PubMed: 9409151]
37. Winter SE, Winter MG, Xavier MN, Thiennimitr P, Poon V, Keestra AM, Laughlin RC, Gomez G, Wu J, Lawhon SD, et al. (2013). Host-derived nitrate boosts growth of E. coli in the inflamed gut. Science 339, 708–711. 10.1126/science.1232467. [PubMed: 23393266]
38. Loy A, Pfann C, Steinberger M, Hanson B, Herp S, Brugiroux S, Gomes Neto JC, Boekschoten MV, Schwab C, Urich T, et al. (2017). Lifestyle and Horizontal Gene Transfer-Mediated Evolution of Mucispirillum schaedleri, a Core Member of the Murine Gut Microbiota. mSystems 2. 10.1128/mSystems.00171-16.
39. Wolf PG, Biswas A, Morales SE, Greening C, and Gaskins HR (2016). H2 metabolism is widespread and diverse among human colonic microbes. Gut Microbes 7, 235–245. 10.1080/19490976.2016.1182288. [PubMed: 27123663]
40. Kraemer JT, and Bagley DM (2006). Supersaturation of dissolved H(2) and CO (2) during fermentative hydrogen production with N(2) sparging. Biotechnol Lett 28, 1485–1491. 10.1007/s10529-006-9114-7. [PubMed: 16955354]
41. Durack J, and Lynch SV (2019). The gut microbiome: Relationships with disease and opportunities for therapy. J Exp Med 216, 20–40. 10.1084/jem.20180448. [PubMed: 30322864]
42. Burkitt DP, Walker AR, and Painter NS (1972). Effect of dietary fibre on stools and the transit-times, and its role in the causation of disease. Lancet 2, 1408–1412. 10.1016/s0140-6736(72)92974-1. [PubMed: 4118696]
43. Hall AB, Yassour M, Sauk J, Garner A, Jiang X, Arthur T, Lagoudas GK, Vatanen T, Fornelos N, Wilson R, et al. (2017). A novel Ruminococcus gnavus clade enriched in inflammatory bowel disease patients. Genome Med 9, 103. 10.1186/s13073-017-0490-5. [PubMed: 29183332]
44. Svolos V, Hansen R, Nichols B, Quince C, Ijaz UZ, Papadopoulou RT, Edwards CA, Watson D, Alghamdi A, Brejnrod A, et al. (2019). Treatment of Active Crohn's Disease With an Ordinary Food-based Diet That Replicates Exclusive Enteral Nutrition. Gastroenterology 156, 1354–1367 e1356. 10.1053/j.gastro.2018.12.002. [PubMed: 30550821]
45. Lloyd-Price J, Arze C, Ananthakrishnan AN, Schirmer M, Avila-Pacheco J, Poon TW, Andrews E, Ajami NJ, Bonham KS, Brislawn CJ, et al. (2019). Multi-omics of the gut microbial ecosystem in inflammatory bowel diseases. Nature 569, 655–662. 10.1038/s41586-019-1237-9. [PubMed: 31142855]
46. Joossens M, Huys G, Cnockaert M, De Preter V, Verbeke K, Rutgeerts P, Vandamme P, and Vermeire S (2011). Dysbiosis of the faecal microbiota in patients with Crohn's disease and their unaffected relatives. Gut 60, 631–637. 10.1136/gut.2010.223263. [PubMed: 21209126]
47. Raygoza Garay JA, Turpin W, Lee SH, Smith MI, Goethel A, Griffiths AM, Moayyedi P, Espin-Garcia O, Abreu M, Aumais GL, et al. (2023). Gut Microbiome Composition Is Associated With Future Onset of Crohn's Disease in Healthy First-Degree Relatives. Gastroenterology 165, 670–681. 10.1053/j.gastro.2023.05.032. [PubMed: 37263307]
48. Zhu W, Winter MG, Byndloss MX, Spiga L, Duerkop BA, Hughes ER, Buttner L, de Lima Romao E, Behrendt CL, Lopez CA, et al. (2018). Precision editing of the gut microbiota ameliorates colitis. Nature 553, 208–211. 10.1038/nature25172. [PubMed: 29323293]
49. Velcich A, Yang W, Heyer J, Fragale A, Nicholas C, Viani S, Kucherlapati R, Lipkin M, Yang K, and Augenlicht L (2002). Colorectal cancer in mice genetically deficient in the mucin Muc2. Science 295, 1726–1729. 10.1126/science.1069094. [PubMed: 11872843]
50. Hoskins LC, Agustines M, McKee WB, Boulding ET, Kriaris M, and Niedermeyer G (1985). Mucin degradation in human colon ecosystems. Isolation and properties of fecal strains that

degrade ABH blood group antigens and oligosaccharides from mucin glycoproteins. J Clin Invest 75, 944–953. 10.1172/JCI111795. [PubMed: 3920248]

51. Johansson ME, and Hansson GC (2012). Preservation of mucus in histological sections, immunostaining of mucins in fixed tissue, and localization of bacteria with FISH. Methods Mol Biol 842, 229–235. 10.1007/978-1-61779-513-8_13. [PubMed: 22259139]
52. Chassaing B, Aitken JD, Malleshappa M, and Vijay-Kumar M (2014). Dextran sulfate sodium (DSS)-induced colitis in mice. Curr Protoc Immunol 104, 15 25 11–15 25 14. 10.1002/0471142735.im1525s104.
53. Herp S, Brugiroux S, Garzetti D, Ring D, Jochum LM, Beutler M, Eberl C, Hussain S, Walter S, Gerlach RG, et al. (2019). Mucispirillum schaedleri Antagonizes Salmonella Virulence to Protect Mice against Colitis. Cell Host Microbe 25, 681–694 e688. 10.1016/j.chom.2019.03.004. [PubMed: 31006637]
54. Bergstrom A, Kristensen MB, Bahl MI, Metzdorff SB, Fink LN, Frokiaer H, and Licht TR (2012). Nature of bacterial colonization influences transcription of mucin genes in mice during the first week of life. BMC Res Notes 5, 402. 10.1186/1756-0500-5-402. [PubMed: 22857743]
55. Liu J, Li P, Wang L, Li M, Ge Z, Noordam L, Lieshout R, Verstegen MMA, Ma B, Su J, et al. (2021). Cancer-Associated Fibroblasts Provide a Stromal Niche for Liver Cancer Organoids That Confers Trophic Effects and Therapy Resistance. Cell Mol Gastroenterol Hepatol 11, 407–431. 10.1016/j.jcmgh.2020.09.003. [PubMed: 32932015]
56. Chen L, Zhai Y, Wang Y, Fearon ER, Nunez G, Inohara N, and Cho KR (2021). Altering the Microbiome Inhibits Tumorigenesis in a Mouse Model of Oviductal High-Grade Serous Carcinoma. Cancer Res 81, 3309–3318. 10.1158/0008-5472.CAN-21-0106. [PubMed: 33863776]
57. Gomes-Neto JC, Mantz S, Held K, Sinha R, Segura Munoz RR, Schmaltz R, Benson AK, Walter J, and Ramer-Tait AE (2017). A real-time PCR assay for accurate quantification of the individual members of the Altered Schaedler Flora microbiota in gnotobiotic mice. J Microbiol Methods 135, 52–62. 10.1016/j.mimet.2017.02.003. [PubMed: 28189782]
58. Kitamoto S, Nagao-Kitamoto H, Jiao Y, Gillilland MG 3rd, Hayashi A, Imai J, Sugihara K, Miyoshi M, Brazil JC, Kuffa P, et al. (2020). The Intermucosal Connection between the Mouth and Gut in Commensal Pathobiont-Driven Colitis. Cell 182, 447–462 e414. 10.1016/j.cell.2020.05.048. [PubMed: 32758418]
59. Seregin SS, Golovchenko N, Schaf B, Chen J, Pudlo NA, Mitchell J, Baxter NT, Zhao L, Schloss PD, Martens EC, et al. (2017). NLRP6 Protects Il10(−/−) Mice from Colitis by Limiting Colonization of Akkermansia muciniphila. Cell Rep 19, 733–745. 10.1016/j.celrep.2017.03.080. [PubMed: 28445725]
60. Caruso R, Ono M, Bunker ME, Nunez G, and Inohara N (2019). Dynamic and Asymmetric Changes of the Microbial Communities after Cohousing in Laboratory Mice. Cell Rep 27, 3401–3412 e3403. 10.1016/j.celrep.2019.05.042. [PubMed: 31189120]
61. Schloss PD, Westcott SL, Ryabin T, Hall JR, Hartmann M, Hollister EB, Lesniewski RA, Oakley BB, Parks DH, Robinson CJ, et al. (2009). Introducing mothur: open-source, platform-independent, community-supported software for describing and comparing microbial communities. Appl Environ Microbiol 75, 7537–7541. 10.1128/AEM.01541-09. [PubMed: 19801464]
62. Pruesse E, Quast C, Knittel K, Fuchs BM, Ludwig W, Peplies J, and Glockner FO (2007). SILVA: a comprehensive online resource for quality checked and aligned ribosomal RNA sequence data compatible with ARB. Nucleic Acids Res 35, 7188–7196. 10.1093/nar/gkm864. [PubMed: 17947321]
63. Edgar RC, Haas BJ, Clemente JC, Quince C, and Knight R (2011). UCHIME improves sensitivity and speed of chimera detection. Bioinformatics 27, 2194–2200. 10.1093/bioinformatics/btr381. [PubMed: 21700674]
64. Dereeper A, Guignon V, Blanc G, Audic S, Buffet S, Chevenet F, Dufayard JF, Guindon S, Lefort V, Lescot M, et al. (2008). Phylogeny.fr: robust phylogenetic analysis for the non-specialist. Nucleic Acids Res 36, W465–469. 10.1093/nar/gkn180. [PubMed: 18424797]
65. Langmead B, and Salzberg SL (2012). Fast gapped-read alignment with Bowtie 2. Nat Methods 9, 357–359. 10.1038/nmeth.1923. [PubMed: 22388286]

66. Patro R, Duggal G, Love MI, Irizarry RA, and Kingsford C (2017). Salmon provides fast and bias-aware quantification of transcript expression. Nat Methods 14, 417–419. 10.1038/nmeth.4197. [PubMed: 28263959]

67. Buchfink B, Xie C, and Huson DH (2015). Fast and sensitive protein alignment using DIAMOND. Nat Methods 12, 59–60. 10.1038/nmeth.3176. [PubMed: 25402007]

68. Nurk S, Meleshko D, Korobeynikov A, and Pevzner PA (2017). metaSPAdes: a new versatile metagenomic assembler. Genome Res 27, 824–834. 10.1101/gr.213959.116. [PubMed: 28298430]

69. Sondergaard D, Pedersen CN, and Greening C (2016). HydDB: A web tool for hydrogenase classification and analysis. Sci Rep 6, 34212. 10.1038/srep34212. [PubMed: 27670643]

70. Luis AS, Jin C, Pereira GV, Glowacki RWP, Gugel SR, Singh S, Byrne DP, Pudlo NA, London JA, Basle A, et al. (2021). A single sulfatase is required to access colonic mucin by a gut bacterium. Nature 598, 332–337. 10.1038/s41586-021-03967-5. [PubMed: 34616040]

71. Kim YG, Sakamoto K, Seo SU, Pickard JM, Gillilland MG 3rd, Pudlo NA, Hoostal M, Li X, Wang TD, Feehley T, et al. (2017). Neonatal acquisition of Clostridia species protects against colonization by bacterial pathogens. Science 356, 315–319. 10.1126/science.aag2029. [PubMed: 28428425]

72. Wolfe RS, and Metcalf WW (2010). A vacuum-vortex technique for preparation of anoxic solutions or liquid culture media in small volumes for cultivating methanogens or other strict anaerobes. Anaerobe 16, 216–219. 10.1016/j.anaerobe.2009.11.005. [PubMed: 20004732]

73. Bronk DA, Roberts QN, Sanderson MP, Canuel EA, Hatcher PG, Mesfioui R, Filippino KC, Mulholland MR, and Love NG (2010). Effluent organic nitrogen (EON): bioavailability and photochemical and salinity-mediated release. Environ Sci Technol 44, 5830–5835. 10.1021/es101115g. [PubMed: 20590151]

Highlights

- Dietary fiber exclusion is beneficial in a spontaneous Crohn's disease-like colitis model
- Fiber exclusion alters the localization of a mucus-dwelling pathobiont, *M. schaedleri*
- Fiber deprivation impairs a critical *M. schaedleri* metabolic pathway
- Pathobiont localization in the intestinal mucus layer is critical for causing disease

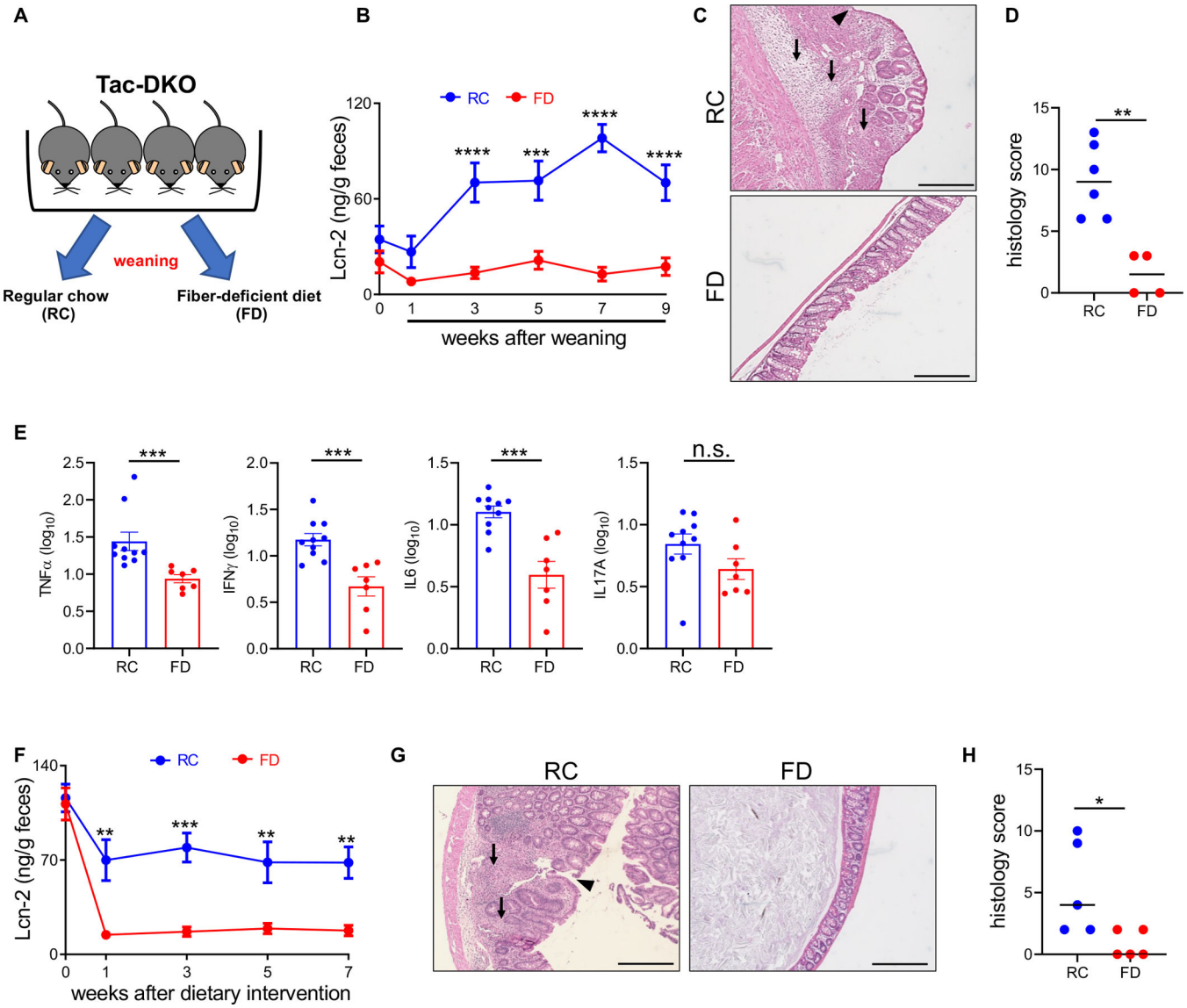

Figure 1. Fiber-deficient diet inhibits intestinal inflammation in Tac-DKO mice.

(A) Schematic representation of the experimental design for feeding strategies. Fecal Lcn-2 levels in Tac-DKO mice fed either the RC or the FD during preventive (B), and therapeutic approach (F). Representative hematoxylin and eosin (H&E)-stained colonic sections from RC- and FD-fed Tac-DKO mice during preventive (C) and therapeutic (G) approach. Scale bar, 200 μm. Arrowhead shows ulcer. Black arrows indicate colonic transmural inflammation. Histology scores of colonic tissue from RC-fed Tac-DKO and FD-fed Tac-DKO mice during preventive (D) and therapeutic (H) approach. (E) Gene expression in colonic tissue of RC-fed and FD-fed Tac-DKO mice was normalized to GAPDH expression. Each symbol represents one mouse. Data are mean ± SEM (B, E and F), or median (D and H); and representative of at least two independent experiments, n= 4–12 per group. **p<0.01; ***p<0.001; ****p<0.0001; n.s. not significant by two-way repeated measures ANOVA followed by Sidak's post-test (B and F), by two-tailed unpaired t-test (E) or by

two-tailed Mann-Whitney U test (**p=0.0095, D; **p=0.0476, H). See also Figure S1; Tables S1 and S7.

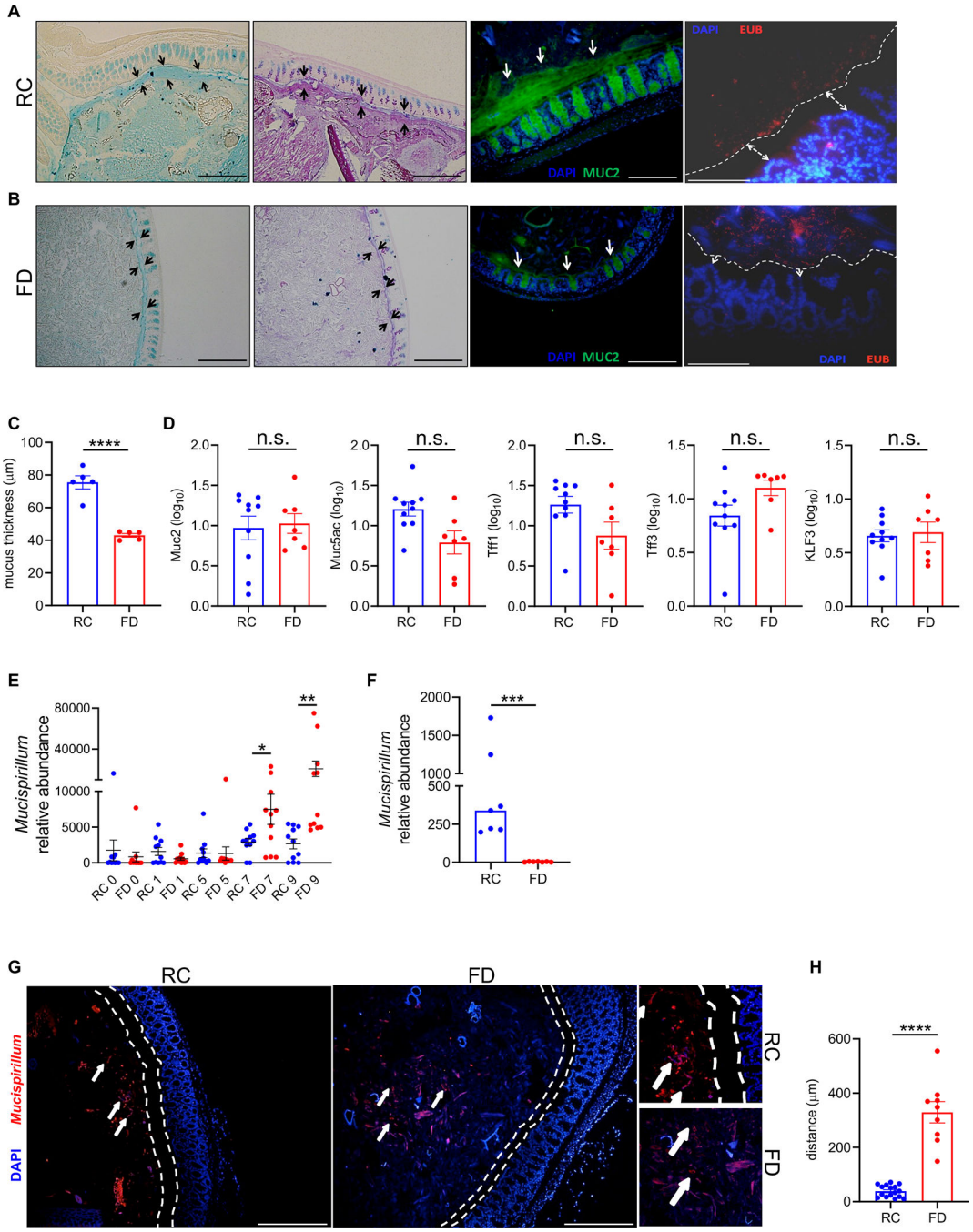

Figure 2. Fiber-deficient diet leads to altered localization of gut pathobiont *Mucispirillum* in Tac-DKO mice.

Alcian blue-stained (first panel from the left) and Alcian blue/PAS-stained (second panel from the left) colonic sections from RC-fed (A) and FD-fed (B) Tac-DKO mice. Opposing black arrows delineate the mucus layer. Scale bars, 200 µm. Immunofluorescence images of colonic sections (third panel from the left) from RC-fed (A) and FD-fed (B) Tac-DKO mice stained with anti-Muc2 antibody (green) and DAPI (blue). White arrows indicate the mucus layer. Scale bars, 200 µm. Fluorescence in situ hybridization (FISH) (right panel) of colonic sections from RC-fed (A) and FD-fed (B) Tac-DKO mice (red, EUB338 probe; blue, DAPI).

Dashed white line and white arrows delineate mucus layer. Scale bars, 100 μm. (C) Colonic mucus layer measurements in RC-fed and FD-fed Tac-DKO mice. (D) Gene expression in colonic tissue of RC-fed and FD-fed Tac-DKO mice was normalized to GAPDH expression. (E) Abundance of *Mucispirillum* in fecal DNA from RC-fed and FD-fed Tac-DKO mice was normalized to the universal 16S rRNA gene. (F) Abundance of *Mucispirillum* in colonic mucus scrapings harvested from RC-fed and FD-fed Tac-DKO mice was normalized to the universal 16S rRNA gene. (G) FISH analysis using *Mucispirillum*-specific probe (red) and DAPI (blue) of colonic sections from RC-fed (left panel) and FD-fed (right panel) Tac-DKO mice. Dashed white lines delineate mucus layer. White arrows indicate *Mucispirillum.* Scale bars, 200 μm. Insets: shows a higher magnification of *Mucispirillum* in proximity to host epithelium in RC-fed animals (top inset), and in the lumen in FD-fed mice (lower inset). (H) Distance from bacterium *Mucispirillum* to the inner mucus layer in RC- or FD-fed Tac-DKO mice.

Each symbol represents one mouse. Data are mean ± SEM (C, D, E and H), or median (F), and representative of at least two independent experiments, n= 5–11 per group. *p< 0.05; **p<0.01; ***p<0.001; ****p<0.0001; n.s. not significant by two-tailed unpaired t-test (C, D and H), by one-way ANOVA followed by Tukey's post-test (E), or by two-tailed Mann-Whitney U test (***p=0.0006, F). See also Figure S2; Table S7.

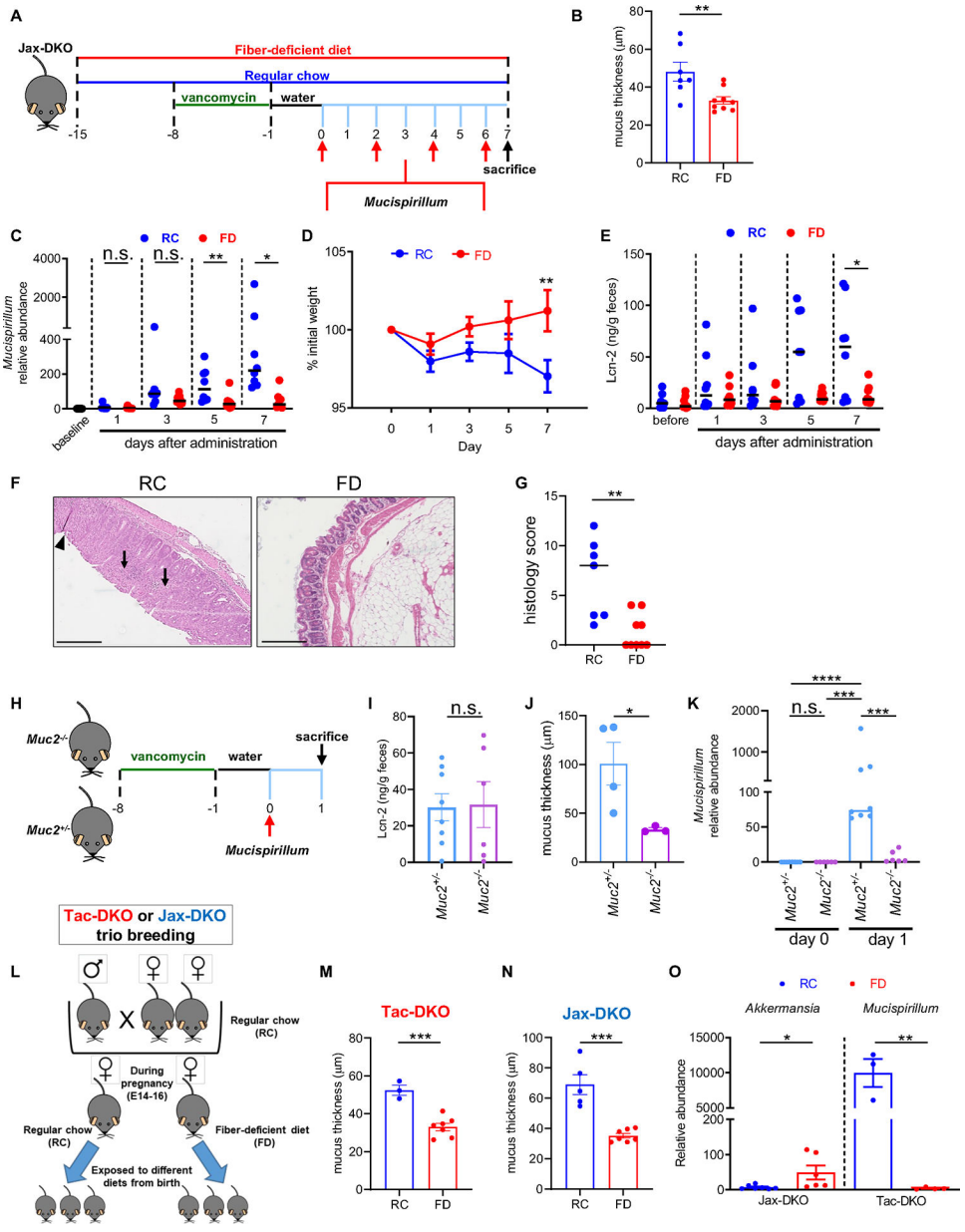

Figure 3. The intestinal mucus layer is critical for *Mucispirillum* intestinal colonization.

(A) Schematic representation of *Mucispirillum* challenge in Jax-DKO mice. (B) Colonic mucus layer measurements in RC-fed and FD-fed Jax-DKO mice. (C) Luminal abundance of *Mucispirillum* prior (baseline) and every other day up to 7 days after bacterial administration in RC-fed and FD-fed Jax-DKO mice was normalized to the universal 16S rRNA gene. (D) Body weight during the 7-day bacterial challenge in RC-fed and FD-fed Jax-DKO mice. (E) Fecal Lcn-2 levels before (day 0) and 7 days after the first *Mucispirillum* oral gavage. (F) Representative H&E-stained colonic sections from *Mucispirillum*-infected Jax-DKO mice fed either RC or the FD. Scale bar, 200 μm. Black arrows indicate colonic inflammatory infiltrate and crypt architectural distortion. (G) Histology scores of colonic tissues from *Mucispirillum*-infected Jax-DKO fed either RC or the FD. (H)

Schematic representation of *Mucispirillum* challenge in *Muc2*$^{-/-}$ mice. (I) Fecal Lcn-2 levels 1 day after the oral gavage in *Muc2*$^{+/-}$ and *Muc2*$^{-/-}$ mice. (J) Colonic mucus thickness measurements in *Mucispirillum*-infected *Muc2*$^{+/-}$ and *Muc2*$^{-/-}$ mice. (K) Luminal Abundance of *Mucispirillum* in in *Muc2*$^{+/-}$ and *Muc2*$^{-/-}$ mice prior (day 0), and 1 day after bacterial administration was normalized to the universal 16S rRNA gene. (L) Schematic representation of the experimental design for trio breeding experiments. Colonic mucus thickness measurements in Tac-DKO (M) and Jax-DKO (N) pups fed either RC or the FD from birth. (O) Abundance of *A. muciniphila* (*Akkermansia*) and *Mucispirillum* in Jax-DKO and Tac-DKO pups, respectively, was normalized to the universal 16S rRNA gene.
Each symbol represents one mouse. Data are mean ± SEM (B, D, I-J, M-O), or median (C, E and K), and representative of at least two independent experiments, n= 3–9 per group. *p< 0.05; **p<0.01; ***p<0.001; ****p<0.0001; n.s. not significant by Kruskal-Wallis test followed by Dunn's post-test (C, E and K), by two-way ANOVA followed by Sidak's post-test (D), by two-tailed Mann-Whitney U test (**p=0.0053, G), or by two-tailed unpaired t-test (**p=0.0081, B; n.s., I; *p=0.0498, J; ***p=0.0006, M; ***p=0.0002, N; **p=0.0424 Jax-DKO, O; **p=0.0018 Tac-DKO, O). See also Figure S3; Table S7.

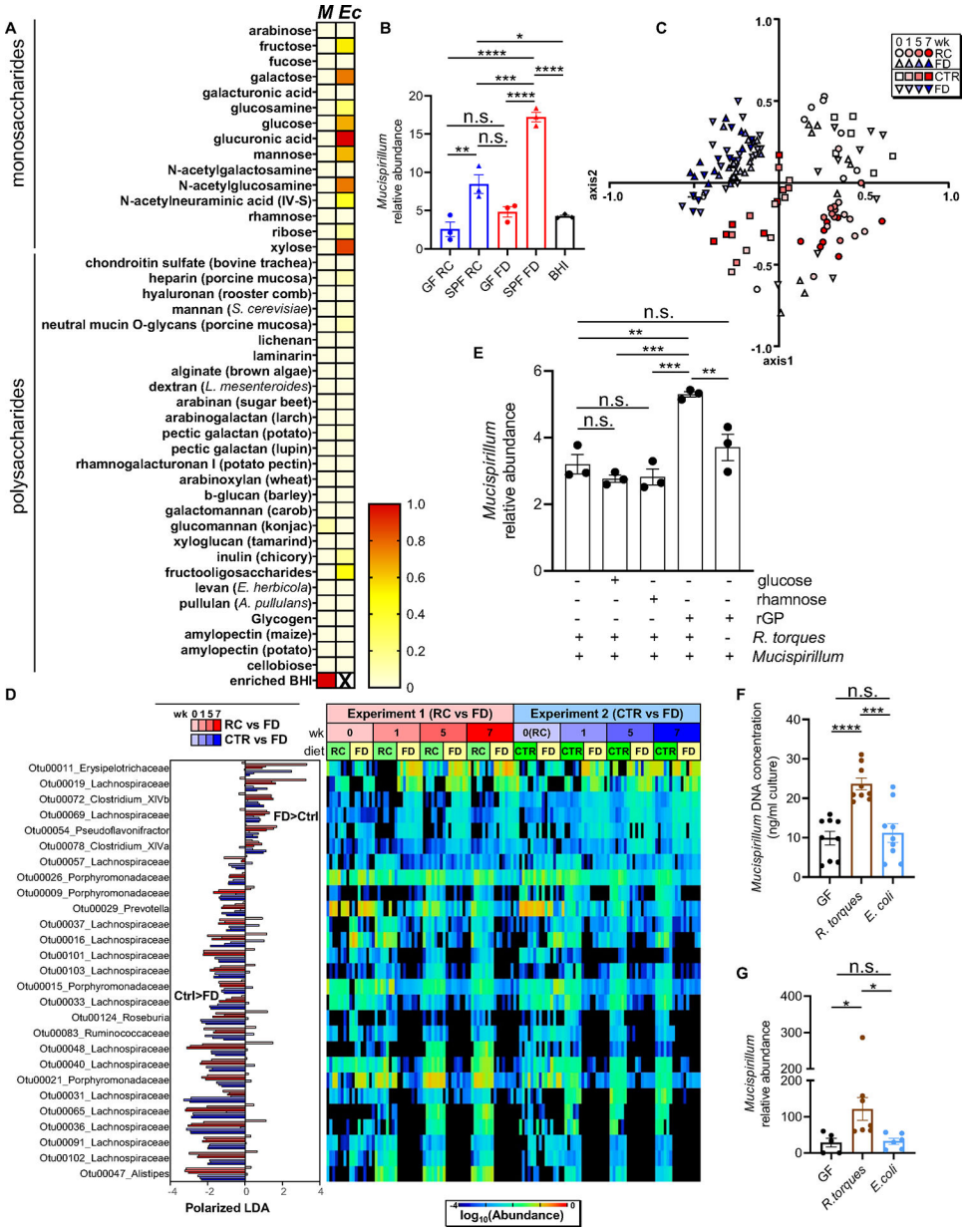

Figure 4. Mucin-degrading microbes promote *Mucispirillum* growth.

(A) Heat map showing normalized growth values of *Mucispirillum* (*M*) or *E. coli* (*Ec*) (enriched BHI, positive control for *Mucispirillum).* (B) *Mucispirillum* growth in the presence of either GF- or SPF-derived supernatants (enriched BHI (BHI), positive control). *Mucispirillum* abundance was normalized to the universal 16S rRNA gene. (C) NMDS plot of θ_{YC} β-diversity indexes of fecal microbiota from Tac-DKO mice fed either RC (circles), CTR (squares) or FD (triangles) for up to 7 weeks. (D) OTUs differentially abundant in fecal microbiota of Tac-DKO mice fed the FD or the control diets (RC or CTR) shown with LDA values of LEfSe with $p<0.05$, false discovery rate <0.05 and maximal abundance cutoff <1%. (E) *Mucispirillum* and *R. torques* co-culture in custom chopped meat broth in the presence of rectal glycoproteins (rGP), glucose or rhamnose. *Mucispirillum*

abundance was normalized to the universal 16S rRNA gene. (F) *Mucispirillum* growth in the presence of supernatants derived from GF, *R. torques*-monocolonized and *E. coli*-monocolonized mice. (G) Abundance of *Mucispirillum* in GF, *R. torques*-monocolonized and *E. coli*-monocolonized mice was normalized to the universal 16S rRNA gene. Each symbol represents one mouse, except for panel B, in which each dot represents data pooled from 3 individual mice. Data are mean ± SEM, representative of at least two independent experiments, n= 5–9 per group. *p< 0.05; **p<0.01; ***p<0.001; ****p<0.0001; n.s. not significant by one-way ANOVA followed by Tukey's post-test. See also Figures S4 and S5; Tables S2, S3 and S7.

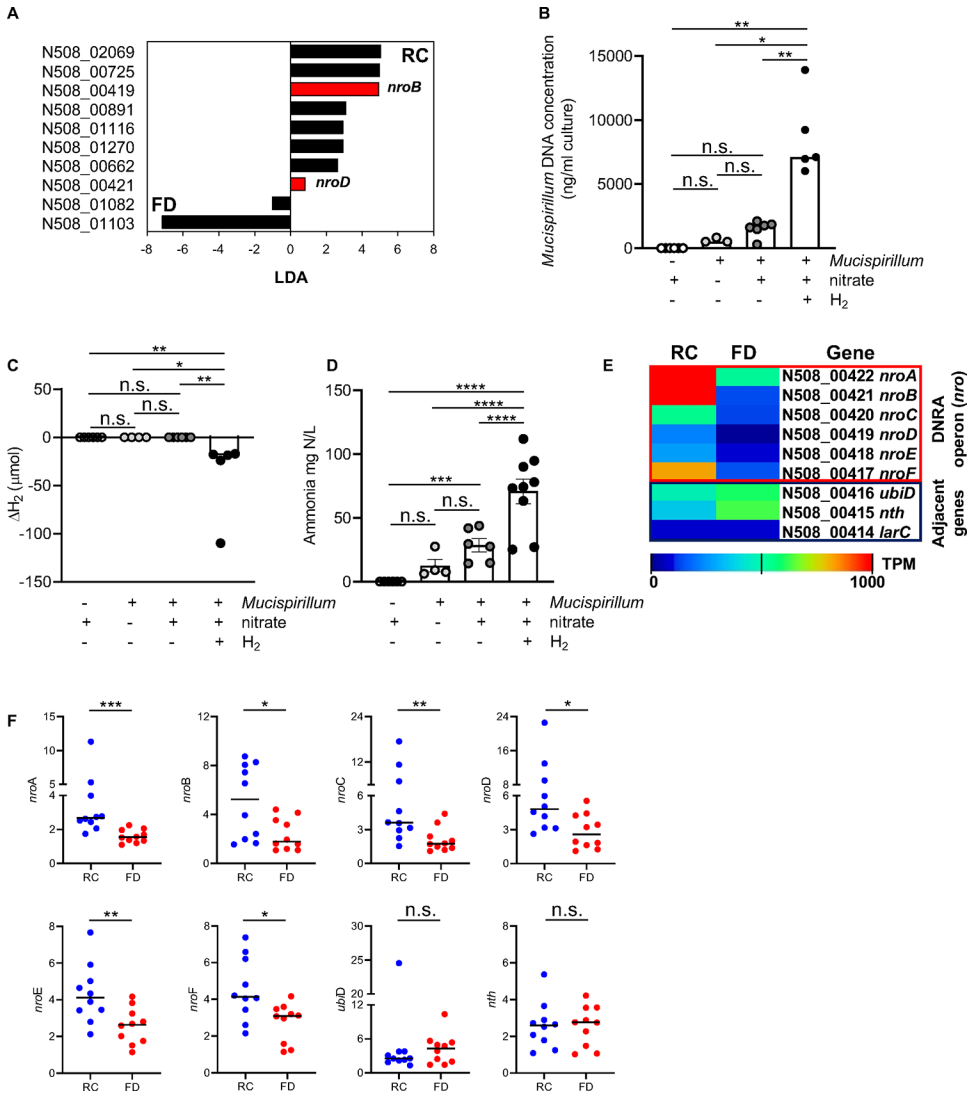

Figure 5. Dietary fiber affects dissimilatory nitrate reduction to ammonium in *Mucispirillum*.

(A) *Mucispirillum* genes differentially expressed in the two groups of diets (RC *vs* FD) shown with LDA values by LEfSe with p<0.05, maximum transcript per million (TPM)>10, and >5-fold difference. Red bars indicate *nroB* and *nroD* genes that encode putative α and δ subunits of the nitrate reductase, respectively. Black bars indicate genes encoding for uncharacterized proteins. *Mucispirillum* was grown in the presence/absence of nitrate (10mM) and H_2 (80%) in enriched BHI and then *Mucispirillum* growth (B), H_2 consumption (C) and ammonium measurements (D) were assessed after three days. (E) Heat map showing the DNRA operon (*nro*) (loci N508_00422-N508_00417) in mucus isolates from RC- or FD-fed Tac-DKO mice (adjacent genes, control). Average transcript levels (log_{10} TPM) in RC- and FD-fed mice. p=not significant. (F) Gene expression in mucus isolates from RC-fed or FD-fed Tac-DKO animals normalized to gap expression.

Each symbol represents one mouse. Data are mean ± SEM (D), or median (B, C and F), and representative of at least two independent experiments, n= 4–10 per group. *p< 0.05; **p<0.01; ***p<0.001; ****p<0.0001; n.s. not significant by Kruskal-Wallis test followed

by Dunn's post-test (B-C), by one-way ANOVA followed by Tukey's post-test (D), by two-tailed unpaired t-test (E), or by two-tailed Mann-Whitney U test (***p=0.0002, *nro*A; *p=0.0355, *nro*B; **p=0.0089, *nro*C; *p=0.0232, *nro*D; **p=0.0068, *nro*E; *p=0.0185, *nro*F; n.s. not significant, *nth* and *ubi*D, F). See also Figure S6; Tables S4 and S7.

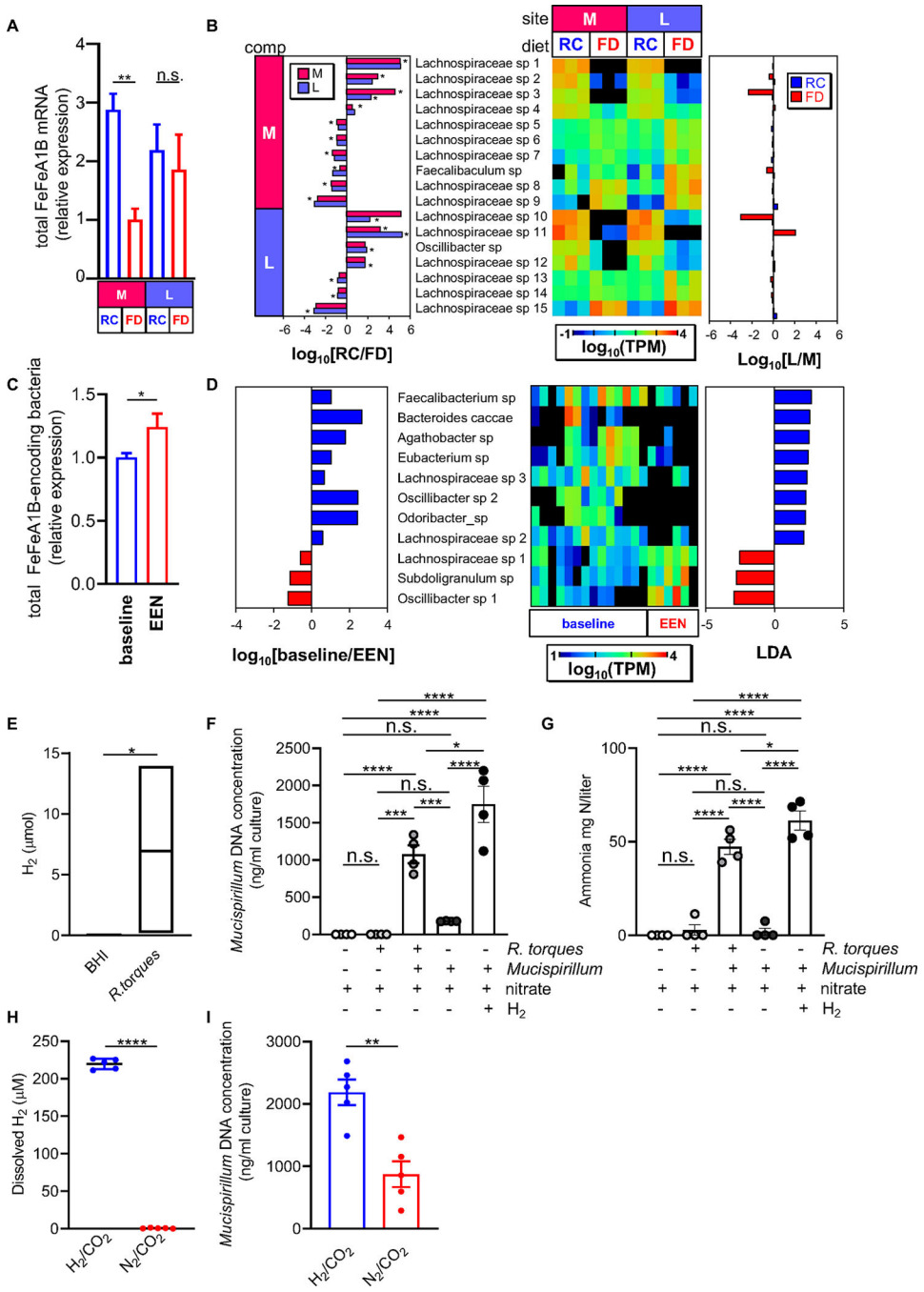

Figure 6. Fiber exclusion alters fermentative H_2 metabolism and interspecies H_2 transfer.

(A) Relative expression level of total FeFe hydrogenase groups A1 and B in mucus (M) and luminal (L) compartments of RC-fed and FD-fed Tac-DKO mice. FeFe Groups A1 and B expression was normalized to 20 housekeeping genes. (B) Genes were selected by comparison between RC and FD at L and M compartments. Microbial species that were differentially abundant in RC *vs* FD group, and in L *vs* M are shown as $\log_{10}$ RC/FD (left panel), $\log_{10}$ TPM (central heat map), and $\log_{10}$ L/M (right panel). (C) Abundance of total bacterial FeFe hydrogenase group A1 and B homologues normalized by the abundance of 20

housekeeping genes in the data obtained from CD patients (Original raw data SRP057027 retrieved from [26]). (D) Specific FeFe A1/B homologues-harboring species with differential abundance between baseline and 1-week EEN treatment (right panel) are shown with heat map (central panel, $\log_{10}$ TPM) and LDA values of LEfSe with $p<0.05$ (left panel). (E) H_2 content in *R. torques* cultures (enriched BHI medium, control). *Mucispirillum* was grown in the presence/absence of *R. torques*, nitrate (10mM) and H_2 (80%) in enriched BHI. *Mucispirillum* growth (F) and ammonium measurements (G) were assessed after three days. Co-cultures of *R. torques* and *Mucispirillum* in bioreactor vessels sparged with a mixed gas containing 20% CO_2 and either 80% N_2 or 80% H_2. (H) Dissolved H_2 concentration at 26.5 hours post-inoculation. (I) *Mucispirillum* growth at day 3 post-inoculation.
Each symbol represents one mouse. Data are mean ± SEM (A, C, F-I), or floating bars show max and min values and line at median (E), and representative of at least two independent experiments, n= 4–5 per group. **p<0.01; ***p<0.001; ****p<0.0001; n.s. not significant by one-way ANOVA followed by Tukey's post-test (A, F-G), by two-tailed Mann-Whitney U test (*p=0.02, C; *p=0.0286, E), or by two-tailed unpaired t-test (****p<0.0001, H; **p=0.0020, I). See also Figure S7; Table S5, S6 and S7.

REAGENT or RESOURCE	SOURCE	IDENTIFIER
Antibodies		
Mucin 2 antibody (C3)	GeneTex	Cat# GTX100664 RRID: AB_1950958
Alexa Fluor 488 goat anti-rabbit IgG	Invitrogen	Cat# A11008; RRID: AB_143165
Alexa Fluor 555-conjugated EUB338 probe	Invitrogen	Johansson et al.[51]
Msc487_correct-2xCy3-conjugated *Mucispirillum* probe	Sigma-Aldrich	Herp et al.[53]
Bacterial and virus strains		
Mucispirillum schaedleri	Dr. Jani L. O'Rourke	Robertson et al.[31]
Escherichia coli K12 strain BW25113	Yale Coli Genetic Stock Center	https://cgsc.biology.yale.edu/
Ruminococcus torques strain VIII	Dr. Eric C. Martens	Hoskins et al.[50]
Chemicals, peptides, and recombinant proteins		
Acid casein peptone	Thermo Fisher Scientific	Cat# BP1424-100
Acetic acid, glacial	Thermo Fisher Scientific	Cat# A38S
Adenine	Sigma-Aldrich	Cat# A2786
Alanine	Sigma-Aldrich	Cat# A7627
Alcian blue	Sigma-Aldrich	Cat# A5268
Alginate	Sigma-Aldrich	Cat# 180947
Agar	BD Difco	Cat# 214010
Ammonium Chloride	Fisher Scientific	Cat# A661-500
Amylopectin from maize	Sigma-Aldrich	Cat# 10120
Arabinose	Sigma-Aldrich	Cat# A3131
Arginine	Sigma-Aldrich	Cat# A8094
Asparagine	Sigma-Aldrich	Cat# A4159
Aspartic Acid	Sigma-Aldrich	Cat# A93100
Barley β-glucan	Megazyme	Cat# P-BGBL
Beef extract	BD Difco	Cat# 212303
Biotin	Sigma-Aldrich	Cat# B4501
Boric acid	Sigma-Aldrich	Cat# B6768
Bovine Serum Albumin	Thermo Fisher Scientific	Cat# BP9703-100
Brain Heart Infusion	BD Difco	Cat# 237500
Brain Heart Infusion (dextrose-free)	MyBiosource	Cat# MBS652861
Calcium chloride	Sigma-Aldrich	Cat# C5670
Calcium pantothenate	Sigma-Aldrich	Cat# P2250
Cellobiose	Sigma-Aldrich	Cat# C7252
Chloroform	Sigma-Aldrich	Cat# 288306
Chondroitin sulfate	Sigma Aldrich	Cat# C9819
Citrate buffer (pH 6.0)	Sigma Aldrich	Cat# C9999
Copper (II) sulfate pentahydrate	Sigma Aldrich	Cat# 209198

REAGENT or RESOURCE	SOURCE	IDENTIFIER
Cyanocobalamin	Sigma Aldrich	Cat# C3607
Cysteine	Sigma Aldrich	Cat# C7352
Cytosine	Sigma Aldrich	Cat# C3506
DAPI (ProLong Gold Antifade reagent)	Invitrogen	Cat# P36931
Dextran	Sigma Aldrich	Cat# D5251
Dextran Sodium Sulfate	MP Biomedical	Cat# 0216011025
Dipotassium phosphate	Sigma Aldrich	Cat# P3786
Disodium succinate	Sigma Aldrich	Cat# W327700
DL-Dithiothreitol	Sigma Aldrich	Cat# D9779
EDTA	Sigma Aldrich	Cat# ED4SS
EDTA solution (pH 8.0)	Thermo Fisher Scientific	Cat# BMA51201
Ethanol	Thermo Fisher Scientific	Cat# BP2818-4
Ferrous sulfate	Sigma Aldrich	Cat# F8048
FITC-dextran	Sigma Aldrich	FD4
Folic acid	Sigma Aldrich	Cat# F7876
Formalin Phosphate (10% buffered)	Thermo Fisher Scientific	Cat# SF100-20
Fructooligosaccharides	Commercial food supply	N/A
Fructose	Sigma Aldrich	Cat# F0127
Fucose	Sigma Aldrich	Cat# F2252
Galactomannan	Megazyme	Cat# P-GALML
Galactose	Sigma Aldrich	Cat# G0750
Galacturonic acid	Sigma Aldrich	Cat# 73960
Glucomannan	Megazyme	Cat# P-GLCML
Glucosamine	Sigma Aldrich	Cat# G4875
Glucose	Sigma Aldrich	Cat# G8270
Glucuronic acid	Sigma Aldrich	Cat# G8645
Glutamic Acid	Sigma Aldrich	Cat# G1501
Glutamine	Sigma Aldrich	Cat# G8540
Glycerol	Thermo Fisher Scientific	Cat# BP229-4
Glycine	Sigma Aldrich	Cat# G8898
Glycogen	Sigma Aldrich	Cat# G0885
Goat serum	Thermo Fisher Scientific	Cat# 16210-064; Lot# 2226570
Guanine	Sigma Aldrich	Cat# G11950
Guanidine hydrochloride	Sigma Aldrich	Cat# 50950
Hematin	Sigma Aldrich	Cat# H3281
Heparin	Sigma Aldrich	Cat# H0777
Histidine	Sigma Aldrich	Cat# H8000
Horse serum	Thermo Fisher Scientific	Cat# 16050-122; Lot# 2540511
Hydrochloric Acid	Thermo Fisher Scientific	Cat# A144-212

REAGENT or RESOURCE	SOURCE	IDENTIFIER
Hyaluronic acid	Sigma Aldrich	Cat# H5388
Inulin	Sigma Aldrich	Cat# I2255
Iodoacetamide	Sigma Aldrich	Cat# I6125
Iron(II) sulfate heptahydrate	Sigma Aldrich	Cat# 215422
Isoleucine	Sigma Aldrich	Cat# W527602
Lamarin	Sigma Aldrich	Cat# L9634
Larch arabinogalactan	Megazyme	Cat# P-ARGAL
LB agar	Invitrogen	Cat# 22700-041
LB broth	Invitrogen	Cat# L3022
Leucine	Sigma Aldrich	Cat# L8000
Levan	Sigma Aldrich	Cat# L8647
Lichenan	Megazyme	Cat# P-LICHN
Lupin pectic galactan	Megazyme	Cat# P-PGALU
Lysine	Sigma Aldrich	Cat# L5501
Lysozyme	Sigma Aldrich	Cat# L6876
Magnesium sulfate	Sigma Aldrich	Cat# MX0075
Magnesium sulfate heptahydrate	Sigma Aldrich	Cat# M1880
Manganese (II) sulfate monohydrate	Sigma Aldrich	Cat# M8179
Mannan	Sigma Aldrich	Cat# M7504
Mannose	Sigma Aldrich	Cat# M4625
Menadione	Sigma Aldrich	Cat# M5625
Methanol	Sigma Aldrich	Cat# 322415
Methionine	Sigma Aldrich	Cat# M9625
Mucin O-glycans (porcine gastric mucosa)	Dr. Eric C. Martens	N/A
M9 minimal salt	Sigma Aldrich	Cat# M6030
N-acetyl galactosamine	Sigma Aldrich	Cat# A2795
N-acetyl glucosamine	Sigma Aldrich	Cat# A3286
N-acetyl neuraminic acid	Sigma Aldrich	Cat# A0812
Newborn Calf serum	Thermo Fisher Scientific	Cat# 16010-159; Lot#2394148
Nicotinic acid	Sigma Aldrich	Cat# N4126
Nickel (II) chloride hexahydrate	Sigma Aldrich	Cat# 654507
p-Aminobenzoic acid	Sigma-Aldrich	Cat# A9878
Pancreatic digest of casein	Sigma Aldrich	Cat# 70169
PAS staining kit	Sigma-Aldrich	Cat# 95B-1KT
PBS	Thermo Fisher Scientific	Cat# 10010-023
Phenol solution	Thermo Fisher Scientific	Cat# A931L
Phenol:Chloroform:Isoamyl Alcohol (ph: 4.5)	Thermo Fisher Scientific	Cat# AM9722
Phenylalanine	Sigma Aldrich	Cat# P2126
Potato amylopectin	Sigma Aldrich	Cat# 10118

REAGENT or RESOURCE	SOURCE	IDENTIFIER
Potato pectic galactan	Megazyme	Cat# P-GAPT
Proline	Sigma Aldrich	Cat# P5607
Pullulan	Sigma Aldrich	Cat# P4516
Pyridoxine HCl	Sigma Aldrich	Cat# P9755
Resazurin	Sigma Aldrich	Cat# R7017
rhamnose	Sigma Aldrich	Cat# R3875
Rhamnogalacturonan I	Megazyme	Cat# P-RHAM1
Riboflavin	Sigma Aldrich	Cat# R7649
Ribose	Sigma Aldrich	Cat# R7500
SDS	Thermo Fisher Scientific	Cat# BP166-500
Serine	Sigma Aldrich	Cat# 84959
Sheep serum	Sigma-Aldrich	Cat# S2263; Lot# 21H266
Sodium acetate buffer solution (pH 5.2)	Sigma Aldrich	Cat# S7899
Sodium chloride	Sigma Aldrich	Cat# S7653
Sodium citrate dihydrate	Thermo Fisher Scientific	Cat# S279-500
Sodium hydroxide	Thermo Fisher Scientific	Cat# S318-100
Sodium hypochlorite	Clorox	Cat# US001237
Sodium molybdate dihydrate	Sigma Aldrich	Cat# M1651
Sodium nitrate	Sigma Aldrich	Cat# S5506
Sodium nitroprusside dihydrate	Fisher Scientific	Cat# ICN15206125
Sodium phosphate monobasic	Sigma Aldrich	Cat# S8282
Sulfuric acid	Sigma Aldrich	Cat# 84736
Sugar beet arabinan	Megazyme	Cat# P-ARAB
Tamarind xyloglucan	Megazyme	Cat# P-XYGLN
Thiamine HCl	Sigma Aldrich	Cat# T4625
Thioctic acid	Sigma Aldrich	Cat# T5625
Threonine	Sigma Aldrich	Cat# T8625
Thymine	Sigma Aldrich	Cat# T0895
Tris	Thermo Fisher Scientific	Cat# BP152-10
Tris-HCL (pH8)	Thermo Fisher Scientific	Cat# BP1758-500
Trypsin from porcine pancreas	Sigma Aldrich	Cat# T4799
Tryptophan	Sigma Aldrich	Cat# T0254
Tyrosine	Sigma Aldrich	Cat# T3754
Uracil	Sigma Aldrich	Cat# U1128
Valine	Sigma Aldrich	Cat# V0500
Vancomycin	Xellia Pharmaceuticals	NDC#70594-048-01
Wheat arabinoxylan	Megazyme	Cat# P-WAXYL
Xylenes	Thermo Fisher Scientific	Cat# X3S-4
Xylose	Sigma Aldrich	Cat# X3877

REAGENT or RESOURCE	SOURCE	IDENTIFIER
Yeast extract	Sigma Aldrich	Cat# 92144
Zinc sulfate heptahydrate	Sigma Aldrich	Cat# Z0251
2-Mercaptoethanol	Sigma Aldrich	Cat# M3148
Critical commercial assays		
E.Z.N.A.Total RNA Kit I	OMEGA	Cat# R6834-02
E.Z.N.A. Stool DNA Kit	OMEGA	Cat# D4015-02
TrueVIEW® Autofluorescence	Vector Laboratories	Cat# SP-8400
High-Capacity RNA-to-cDNA Kit	Thermo Fisher Scientific	Cat# 4387406
Radiant™ SYBR Green qPCR Kit	Alkali Scientific	Cat# QS1050
RNeasy Mini Kit	QIAGEN	Cat# 74134
RNeasy Micro Kit	QIAGEN	Cat# 74004
Mouse Lipocalin-2/NGAL DuoSet ELISA kit	R & D Biosystems	Cat# DY1857
NEBNext® Ultra™ II Directional RNA Library Prep Kit for Illumina	New England BioLabs	Cat# E7760L
Ribo depletion Module NEBNext rRNA Human/ Mouse/Rat	New England BioLabs	Cat# E6310X
NEBNext rRNA Depletion Kit Bacteria	New England BioLabs	Cat# E7850X
NEBNext Multiplex Oligos for Illumina Unique dual	New England BioLabs	Cat# E6440L
Deposited data		
16S rRNA and RNA sequencing data	This study	BioProject: PRJNA984252
Other		
PowerBead Tubes, garnet (0.70 mm)	QIAGEN	Cat# 13123-50
Fiber-Free diet	Envigo	Cat# TD.130343
Custom CTR diet	Envigo	Cat# TD.190428
Laboratory Autoclavable Rodent Diet - 5LOD	LabDiet	Cat# 3005659-220
Laboratory Autoclavable Rodent Breeder Diet - 5013	LabDiet	Cat# 0006529
Experimental models: Organisms/strains		
Mouse: C57BL/6J: WT	The Jackson Laboratory	JAX: 000664
Mouse: C57BL/6NTac: WT	Taconic Biosciences	B6-F; B6-M
Mouse: *Nod2*$^{-/-}$-*Cybb*$^{-/-}$		Caruso et al.[13]
Mouse: *Muc2*$^{-/-}$	Dr. Eric C. Martens	Velcich et al.[49]
Oligonucleotides		
See Table S7		
Software and algorithms		
Bowtie2	Langmead et al.[65]	https://bowtie-bio.sourceforge.net/bowtie2/index.shtml
Morpheus	N/A	https://software.broadinstitute.org/morpheus/
Aperio ImageScope v 12.1.0.5029	Aperio Technologies, Inc.	https://www2.leicabiosystems.com/

REAGENT or RESOURCE	SOURCE	IDENTIFIER
Mothur (v.1.40.5)	Schloss et al.[61]	https://mothur.org/
UCHIME	Edgar et al.[63]	https://drive5.com/usearch/manual/uchime_algo.html
SILVA 16S rRNA database release 138	Pruesse et al.[62]	https://www.arb-silva.de/
Phylogeny.fr	Dereeper et al.[64]	https://www.phylogeny.fr/simple_phylogeny.cgi
Prism 9.1.0	GraphPad Software	https://www.graphpad.com/scientific-software/prism/
TreeGraph2	N/A	http://treegraph.bioinfweb.info/
Salmon	Patro et al.[66]	https://salmon.readthedocs.io/en/latest/salmon.html
bcl2fastq2 Conversion Software	Illumina	https://support.illumina.com/downloads/bcl2fastq-conversion-software-v2-20.html
UniProt database	N/A	https://www.uniprot.org/
Diamond	Buchfink et al.[67]	https://gensoft.pasteur.fr/docs/diamond/0.8.22/diamond_manual.pdf
metaSPAdes	Nurk et al.[68]	https://cab.spbu.ru/files/release3.12.0/manual.html
HydDB database	Sondergaard et al.[69]	https://services.birc.au.dk/hyddb/
Gen5™	BioTek	https://www.biotek.com/products/software-robotics-software/gen5-microplate-reader-and-imagersoftware/